Natural xanthones as α-Mangostin induce vasorelaxation via binding to key gating residues in the S6 domain of BK channels

Sönke Cordeiro[1], Robert Patejdl[2], Thomas Baukrowitz[1], Marianne Musinszki[1]*

[1] Institute of Physiology, Christian-Albrechts-University Kiel, Germany

[2] Department of Human Medicine, Health and Medical University Erfurt, Germany

** for correspondence: m.musinszki@physiologie.uni-kiel.de*

Abstract

Polyphenolic compounds are widely explored for health benefits, including hypertension, but their active ingredients, molecular targets, and mechanisms remain poorly defined. We identify the xanthone Mangostin from *Garcinia mangostana* as a potent modulator of several potassium channels, with large-conductance K^+ (BK) channels as its primary target for vasorelaxation. Mangostin activated BK channels as α subunits alone, in complexes with vascular β1 subunits, and in reconstituted BKα/β1–Ca_V nanodomains. It shifted BK voltage activation to more negative potentials by antagonizing channel closure and promoting channel opening without markedly altering Ca^{2+} sensitivity. Docking, competition, single channel analysis and mutagenesis localized the binding site in the pore cavity below the SF, involving gating-critical S6 residues I308, L312, and A316, and suggest that Mangostin stays bound in closed and open states. These findings establish BK channel activation as the core molecular mechanism driving Mangostin's vascular effects and define its structural mode of action, informing nutraceutical safety assessment and BK-targeted drug design.

Keywords

Mangostin, xanthones, VSMC, vasorelaxation, hypertension, BK channel, Slo1, KCa1.1

29 **Abbreviations**

30 β1	regulatory β1-subunit of BK channels
31 BKα	Big Potassium (BK) channel pore-forming α-subunit (Slo1, K_{Ca}1.1, MaxiK)
32 BKα/β1	complex of BKα channel and β1 subunit
33 Ca_v	voltage-gated Calcium channel
34 hERG	human Ether-a-go-go Related Gene potassium channel
35 IbTx	Iberiotoxin
36 K_{2P}	Tandem-Pore-Domain Potassium channel
37 K_{ir}	inward-rectifier Potassium channel
38 K_v	voltage-gated Potassium channel
39 MD	Molecular Dynamics (simulations)
40 NCA	Negatively Charged Activator, e.g., BL-1249
41 ROMK	Renal Outer Medullary Potassium channel
42 SF	Selectivity Filter
43 SUR	Sulfonylurea Receptor regulatory subunit of K_{ATP} channels
44 THexA	Tetrahexylammonium ion
45 TPA	Tetrapentylammonium ion

46

47

Introduction

Nutraceuticals (superfoods, dietary supplements, and traditional remedies) promise a plethora of health benefits that are usually not definitely proven by clinical studies. Well-known examples are resveratrol present in grapes and red wine (Jang *et al.*, 1997; Brown *et al.*, 2024), carotenes and tocopherols (Alpha-Tocopherol, Beta Carotene Cancer Prevention Study Group, 1994; Hennekens *et al.*, 1996; Xin *et al.*, 2022), or the recent resurgence of quercetin (Lee *et al.*, 2021; Di Pierro *et al.*, 2023). In evaluating clinical relevance and explore pharmacological opportunities of such phytochemicals, obstacles are often the identification of the biologically active substance in complex matrices of plant secondary metabolites and the lack of a definite cellular determinant that could link a biologically active substance to a physiological process. However, a clear molecular target and mechanism of action that can explain its effects is the prerequisite to further drug development.

Natural polyphenols are known to modulate diverse potassium (K^+) channel families. For example, various members of the flavonoid subgroup activate K_{Ca} (BK) channels as well as several K_v, K_{ir}, and K_{2P} channels, including TREK-1 channels ((Gierten *et al.*, 2008; Nardi and Olesen, 2008; Kim, Kang and Han, 2011); for a comprehensive review see (Richter-Laskowska *et al.*, 2023)). A recent study suggested that α-Mangostin, a xanthone from *Garcinia mangostana,* modulates ion channels and binds in the pore cavity of TREK K_{2P} channels (Kim *et al.*, 2023). α- and γ-Mangostins are the main xanthones found in the mangostane fruit pericarp, whose ethanolic extracts are used as traditional medicine and consumed as nutraceuticals. They are thought to exert a plethora of health-promoting effects, such as cardioprotective (Eisvand *et al.*, 2022), analgesic (Kim *et al.*, 2023), antioxidant (Kong, Jia and Jia, 2022), antiinflammatory (Kim *et al.*, 2021), antidiabetic (John *et al.*, 2022), antifibrotic (Li *et al.*, 2019), antimicrobial (Tatiya-Aphiradee, Chatuphonprasert and Jarukamjorn, 2016), and antiproliferative effects (Majdalawieh *et al.*, 2024). Interestingly, very recent research reported that α-Mangostin has antihypertensive properties, and it decreased systolic and diastolic blood pressure in a rat model (Xu *et al.*, 2024). Earlier studies had demonstrated the relaxation of aortic rings upon Mangostin incubation, but remained somewhat contradictory as to the site of action and the molecular target (Chairungsrilerd *et al.*, 1996, 1997; Tep-Areenan and Suksamrarn, 2012). Hence, the molecular mechanism of this antihypertensive effect of Mangostin remains unclear.

Major potassium channels present in vascular smooth muscle are Ca^{2+}-activated BK channels, also known as MaxiK, Slo1 or $K_{Ca}1.1$ channels (Wu and Marx, 2010; Tykocki, Boerman and Jackson, 2017; Pereira da Silva *et al.*, 2022). They are synergistically activated by intracellular calcium (Ca_i^{2+}) and voltage, and they play a crucial role in the regulation of vascular smooth muscle tone, with implications for blood pressure regulation. BK channels act as feedback

regulators which counteract depolarization and balance the elevation of Ca_i^{2+} through voltage-dependent L-type Ca^{2+} channels. The pore-forming BKα subunit is expressed ubiquitously, and tissue specific properties are conveyed by regulatory β-, γ-, and LINGO subunits (Latorre *et al.*, 2017; Gonzalez-Perez and Lingle, 2019; Dudem *et al.*, 2020). In vascular smooth muscle cells, BKα assembles with the β1 subunit, which enhances its apparent Ca_i^{2+} sensitivity, decreases voltage sensitivity (Dworetzky *et al.*, 1996; Brenner *et al.*, 2000; Orio and Latorre, 2005; Li and Yan, 2016), and modulates its pharmacological properties (McManus *et al.*, 1995; Hanner *et al.*, 1997).

Structurally, BK channels are homotetramers consisting of the pore-forming α subunits with 7 transmembrane segments (S0-S6), a linker region, and two intracellular RCK domains. The RCK domains and their interface to the transmembrane segments contain different Ca_i^{2+} binding sites, S1-S4 comprise the voltage sensing domain, and S5 and S6 together with the pore helix constitute the pore domain. Both depolarization or Ca_i^{2+} elevation can open the pore via allosteric mechanisms, and this regulation as well as the modulation by mutations, small molecules, and regulatory subunits can be described well by an allosteric gating model ((Horrigan and Aldrich, 2002; Latorre *et al.*, 2017)). However, the structural determinants that underlie this allosteric modulation remain unclear. The S6 segment has been shown to undergo conformational changes during activation, and several gating sensitive residues as well as modulator binding sites for molecules of surprisingly different chemical structure are known in this pore region or the adjacent linker to the cytoplasmic C-terminus (Nardi and Olesen, 2008; Zhou, Xia and Lingle, 2011; Roy *et al.*, 2012; Hoshi, Xu, *et al.*, 2013; Chen, Yan and Aldrich, 2014; Webb *et al.*, 2015; Hoshi and Heinemann, 2016; Schewe *et al.*, 2019; Rockman, Vouga and Rothberg, 2020a; Gonzalez-Sanabria *et al.*, 2025). Investigations of the activation mechanism indicated that these substances act without directly affecting the voltage- or Ca^{2+} sensory domains, probably by modifying the close interactions of S5 and S6 with the voltage sensor bundle and the gating ring that enable opening of the channel.

Small molecule BK channel activators are promising to treat diverse diseases like fragile X syndrome, overactive bladder, pulmonary hypertension, chronic obstruction, erectile dysfunction, and reperfusion injury; however, no prospective drug successfully completed a phase III trial yet (Bentzen *et al.*, 2014; Barenco-Marins *et al.*, 2023; Ferraguto *et al.*, 2024). Therefore, adding a pharmacophore derived from the xanthone group may aid in developing future drug candidates.

We used a combination of functional studies in cultured cells and vascular tissue as well as molecular docking to show that BK channels are a molecular target of Mangostins and that they mediate vascular relaxation observed upon Mangostin application. BK channels were opened most prominently among the K^+ channel representatives tested and were activated by

α-Mangostin as well as by an extract of the mangosteen pericarp marketed as a nutraceutical. Investigation of the activation mechanism showed that α-Mangostin essentially facilitates BK channel activation by shifting its voltage dependence, modulating gating kinetics, and enhancing the open probability, without changing the Ca_i^{2+} sensitivity. These effects were due to direct binding to the pore-forming BKα subunit. Competition experiments, molecular docking, and scanning mutagenesis identified the binding region in S6 just below the selectivity filter (SF). Mangostin activation was preserved in reconstructed nanodomains with Ca_v channels, which cause local elevation of intracellular Ca_i^{2+}, mimicking the physiological situation in smooth muscle cells. Finally, we show that BK channels specifically mediate relaxation of aortic preparations from mice. Our study explains the molecular activation of BK channels by a natural xanthone and sheds light on the mechanism underlying one of its claimed health benefits.

Results

α-Mangostin particularly activates BKα and BKα/β1 channels

In previous studies, α-Mangostin was shown to activate members of the K_{2P} channel family, while other K^+ channels were inhibited (Kim *et al.*, 2021, 2023). We aimed to obtain a broader pharmacological profile of α-Mangostin in K^+ channels and we investigated members of all six subfamilies of K_{2P} channels as well as representatives of the K_v and K_{ir} channel families. Confirming the previous studies, we observed a strong activation of TREK-1 K_{2P} channels (fold change 10.33 ± 1.64; Fig. 1A and Fig. S1) and inhibition of TRESK K_{2P} channels as well as K_v1.3 channels by ≈50% and ≈60 %, respectively (Fig. 1A, B and Fig. S1). Furthermore, we identified three additional targets of α-Mangostin: strongly inhibited were the K_{2P} members TWIK-1^m (≈88 %), TWIK-2^m (≈50 %), and TASK-3 (≈80 %) (Fig. 1A, B and Fig. S1). In contrast, BK channels were most potently activated, with a fold change of 20.41 ± 2.39 for BKα channels and of 24.42 ± 3.85 for BKα/β1 channels, which is the complex predominantly present in smooth muscle cells of the vasculature (Fig. 1A, C). This suggested that BK channels, especially the BKα/β1 heteromer, could be the molecular target mediating the vasorelaxant Mangostin effects reported in above studies.

The preparations from *Garcinia mangostana* plants that are consumed as 'nutraceuticals' contain an unstandardized mixture of secondary plant metabolites, among them other Mangostin derivatives. Therefore, we also investigated their modulatory effect on TREK-1, BKα and BKα/β1 currents (Fig. 1D). The very similar γ-Mangostin activated BKα channels with slightly higher efficacy (fold change of 38.54 ± 4.8) than TREK-1 and BKα/β1 channels (fold change of 11.35 ± 1 and 29.32 ± 5.03). Interestingly, the dietary supplement (solubilized

155 equivalent to 10 µM α-Mangostin) activated TREK1, BKα and BKα/β1 channels comparably to
156 pure α-/γ-Mangostin (fold change of 9.18 ± 2.74, 19.98 ± 2.99 and 20.92 ± 3.49; Fig. 1D),
157 highlighting that mangostane xanthones retain their activity in such extracts.

158 The application of different α-Mangostin concentrations resulted in a fast and dose-dependent
159 activation of BKα and BKα/β1 channels, with a similar apparent EC_{50} of 3.16 ± 1.13 µM and
160 2.57 ± 1.32 µM, suggesting that the potency of α-Mangostin is not affected by the presence of
161 the β1-subunit (Fig. 1E). However, we frequently noticed a decline of currents at
162 concentrations >12 µM and limited solubility of higher Mangostin concentrations, which may
163 imply that the actual maximal activation could not be reached.

164

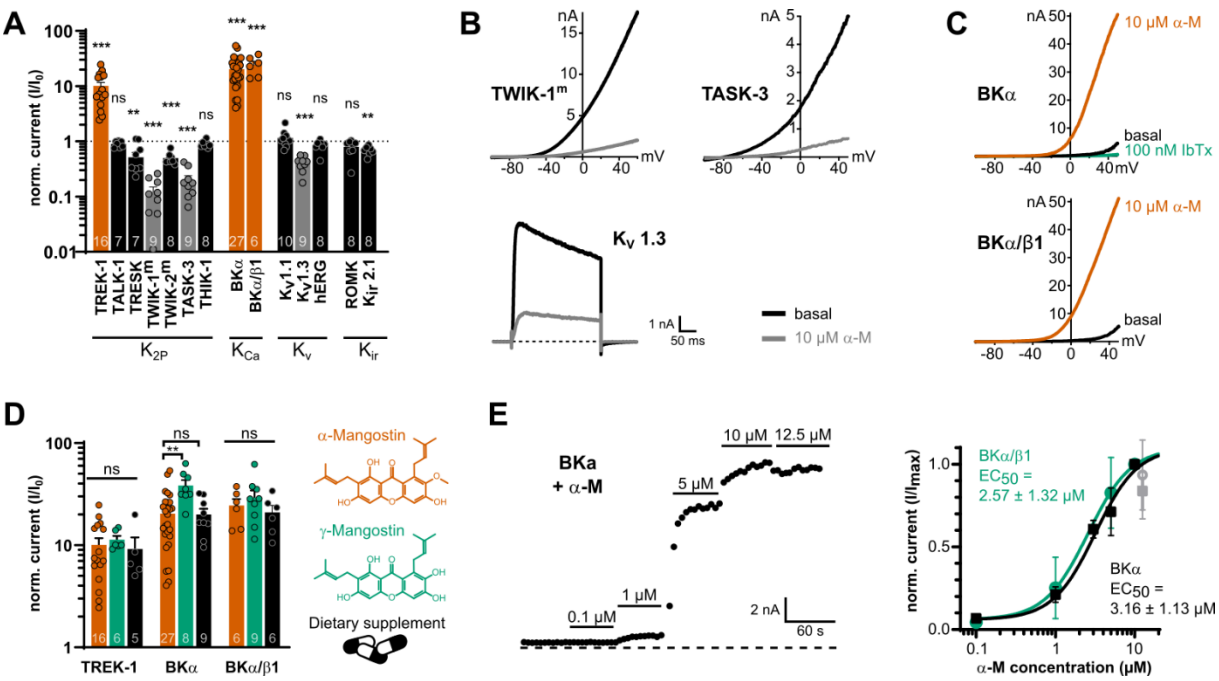

165

166 **Figure 1: Mangostin potently activates BKα and BKα/β1 channels compared to other potassium channel**
167 **representatives. (A)** Current fold change ± SEM of currents of representatives from different potassium channel
168 families upon application of 10 µM α-Mangostin. K_{2P} and K_{Ca} channel currents were recorded with ramp protocols
169 from -100 mV to +50 mV and analyzed at +40 mV; K_v1.1 and K_v1.3 channel currents were evoked using a rectangle
170 pulse to +40 mV, and hERG currents were recorded with a rectangle pulse to +60 mV followed by hyperpolarization
171 to -120 mV, which was analyzed. K_{ir} channels were recorded using ramp protocols from -150 mV to +50 mV, and
172 currents were analyzed at -140mV. All measurements were made in transiently transfected HEK293 cells in
173 physiological potassium gradients with 100 nM intracellular free Ca^{2+} with a holding potential of -80 mV. TWIK-1^m
174 and TWIK-2^m denote channels where the retrieval motif was removed to improve membrane expression, and
175 intracellular K^+ was exchanged for Rb^+ to enhance currents. (**B**) Representative current traces of channels that
176 were inhibited more than 60 % by 10 µM α-Mangostin. (**C**) Representative current traces of BKα and BKα/β1
177 channels activated by 10 µM α-Mangostin (α-M). (**D**) Current fold change ± SEM after application of α-Mangostin,
178 γ-Mangostin, and a dietary supplement to TREK-1, BKα and BKα/β1 channels. Currents were recorded and
179 analyzed as in (A). **(E)** Representative time course of the dose-dependent activation of BKα channels by increasing
180 concentrations of α-Mangostin (left) and the resulting dose-response-relationships for BKα and BKα/β1 channels

181 (right). Currents were recorded and analyzed as in (A); the grey data point at 12.5 µM was not included in the Hill
182 fit. Data and statistics see Tables S1 and S2.

183

184 *α-Mangostin shifts the voltage activation of BKα and BKα/β1 channels to more negative values*

185 Having established the prominent activation of BKα and BKα/β1 channels by α-Mangostin, we
186 wanted to gain more insight into its activation mechanism. The open probability of BK channels
187 is controlled by voltage signals, calcium signals, or shift of the closed-open equilibrium (e.g. by
188 mutations or modulators), and the current further depends on the single channel amplitude and
189 the time the channel adopts an open conductive state. We therefore investigated these aspects
190 of BK channel gating in macroscopic and single-channel measurements.

191 As we already observed in the ramp measurements, the threshold of BK voltage activation
192 was shifted to more negative potentials upon α-Mangostin application (Fig. 1C). Therefore, we
193 first examined if α-Mangostin affects the voltage activation of BK channels. We used a step
194 protocol over a range of potentials followed by a repolarization step to elicit tail currents in
195 symmetrical bi-ionic conditions where intracellular K^+ was replaced with Cs^+ to reduce the
196 strong outward currents in whole-cell experiments (Fig. 2A; Cs^+ does not alter voltage
197 activation (Piskorowski and Aldrich, 2006)). We quantified the change in voltage activation
198 induced by α-Mangostin by calculating the voltage of half-maximal activation ($V_{½}$) from the
199 Boltzmann fit of conductance-voltage (GV) relationships (Fig. 2B). The application of 10 µM α-
200 Mangostin caused a substantial left-shift of the $V_{½}$ by 53.08 ± 4.9 mV in BKα channels (from
201 110.45 ± 2.69 mV to 57.37 ± 3.6 mV). This effect was even more pronounced in smooth
202 muscle-like BKα/β1 channels, where $V_{½}$ shifted by 82.42 ± 4.96 mV to more hyperpolarized
203 voltages (from 147.25 ± 5.66 mV to 64.83 ± 4.25 mV). The slope of the Boltzmann fit was not
204 different before and after α-Mangostin activation in both channels (Fig. 2B, insets). Hence,
205 BKα and BKα/β1 channels already opened at less depolarized voltages in the presence of α-
206 Mangostin, whereas voltage activation itself was not affected.

207

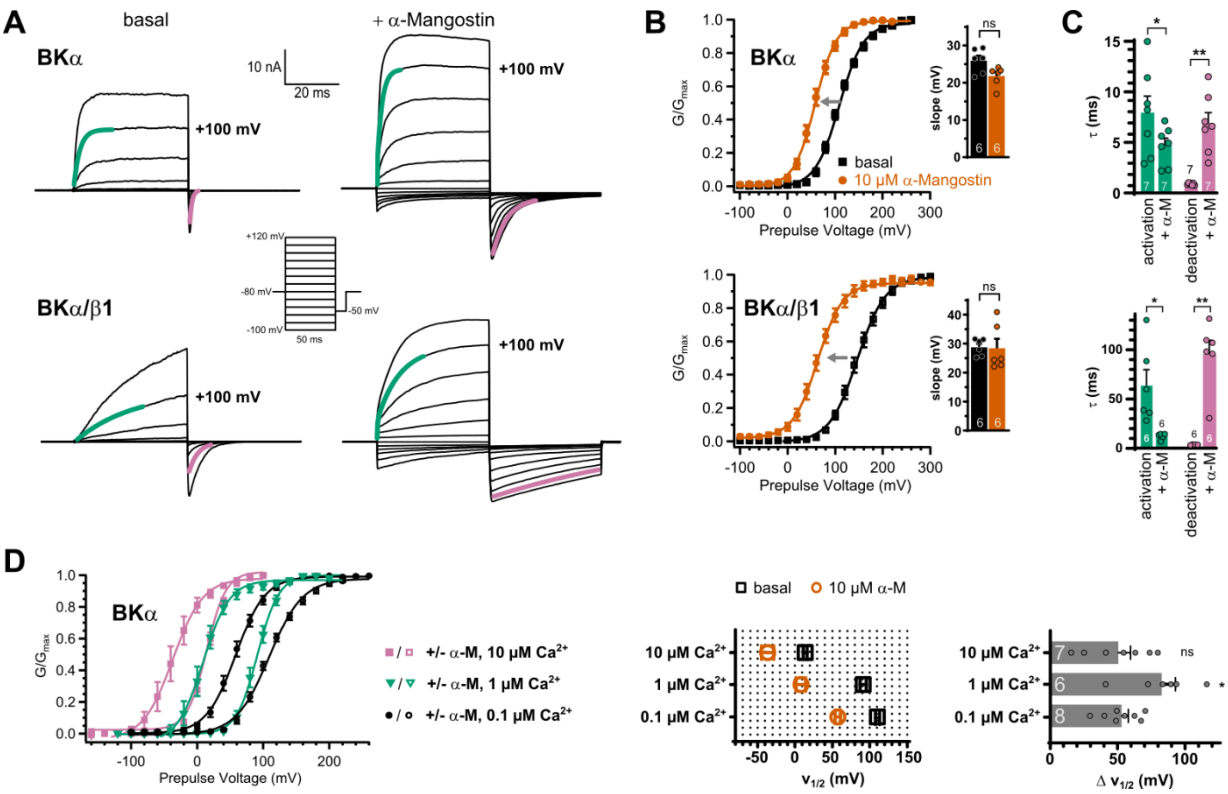

Figure 2: Effects of α-Mangostin on BKα and BKα/β1 channel gating. (A) Representative current traces for BKα and BKα/β1 channels before and after activation by 10 μM α-Mangostin. Cells were measured in symmetrical 140 mM bi-ionic conditions with 140 mM Cs^+ as the intracellular ion and 100 nM free Ca_i^{2+}. Currents were elicited by a family of rectangle pulses from -100 mV to up to +300 mV in 20 mV increments from a holding potential of -80 mV, followed by repolarization to -50 mV to elicit inward tail currents. **(B)** GV-relationships for BKα and BKα/β1 channels in the basal state and activated by 10 μM α-Mangostin, derived from tail current analysis of recordings as in (A). The grey arrow illustrates the left-shift of voltage activation caused by α-Mangostin and the inset shows the slope ± SEM of the Boltzmann fits. **(C)** Activation and deactivation kinetics of BKα and BKα/β1 channels in the basal state and after activation by 10 μM α-Mangostin. The τ ± SEM of activation/deactivation was determined from exponential fits to the current traces at +100 mV, as shown by the green and purple colored lines in panel (A). **(D)** GV-relationships of BKα channels in different free Ca_i^{2+} concentrations before and after activation by 10 μM α-Mangostin, derived from tail current analysis as above. Pulse voltages were -100 mV to +300 mV/ repolarization to -50 mV from a holding potential of -80 mV for 100 nM free Ca_i^{2+}, -120 mV to +200 mV/ repolarization to -50 mV from a holding potential of -80 mV for 1 μM free Ca_i^{2+}, and -160 mV to +100 mV/ repolarization to -80 mV from a holding potential of -120 mV for 10 μM free Ca_i^{2+}, in symmetrical 140 mM bi-ionic conditions with 140 mM Cs^+ as the intracellular ion. The $V_{½}$ values ± SEM before and after α-Mangostin application and the resulting shifts (Δ $V_{½}$ ± SEM) are shown in the bar graphs. Data and statistics see Tables S3 – S5.

α-Mangostin predominantly affects deactivation of BKα and BKα/β1 channels

An inspection of the currents elicited by the families of rectangle pulses shows that gating kinetics are altered in the α-Mangostin activated state (Fig. 2A). The shift in $V_{½}$ towards more negative potentials upon α-Mangostin activation could be caused either by an acceleration of channel activation, or by a slowing down of channel deactivation, or a combination of both. We

232 therefore analyzed the kinetics of activation and deactivation by fitting monoexponential
233 functions to the time course of outward and tail currents for the +100 mV pulse to obtain their
234 time constants (τ). BKα channels are characterized by fast activating current and a fast
235 deactivation visible as decay of the tail current, while the presence of the β1 subunit slows
236 these kinetics down (Fig. 2A, bottom; (Dworetzky *et al.*, 1996)). After application of 10 μM α-
237 Mangostin, activation of BKα channels was moderately accelerated (1.7-fold) with a τ of
238 activation of 7.96 ± 1.64 ms before and 4.71 ± 0.71 ms afterwards, while the τ for deactivation
239 at -50 mV increased ≈7-fold from 0.9 ± 0.04 ms to 6.85 ± 1.11 ms (Fig. 2C). Again, this effect
240 was more pronounced in the smooth muscle-like BKα/β1 channels, where activation was more
241 that 5-fold faster with τ values of 63.76 ± 16.03 ms before and 12.36 ± 1.20 ms after α-
242 Mangostin application. Deactivation kinetics were most affected with a substantial ≈27-fold
243 increase in τ from 3.60 ± 0.16 ms to 95.6 ± 13.99 ms (Fig. 2C). These results suggest that the
244 mechanism of α-Mangostin action differentially affects gating transitions that are associated
245 with activation and deactivation.

246 As BK channels can be massively activated by Ca_i^{2+} under physiological conditions, we further
247 obtained GV-relationships in the basal and in the activated state for higher Ca_i^{2+} concentrations
248 relevant in smooth muscle cells to test if α-Mangostin activation is independent of Ca_i^{2+}
249 concentration (Fig. 2D). α-Mangostin shifted the $V_{½}$ in 10 μM free Ca_i^{2+} by 50.55 ± 9.13 mV to
250 more negative potentials, comparable to the resting state with 0.1 μM free Ca_i^{2+}. However, in
251 1 μM Ca_i^{2+} α-Mangostin the $V_{½}$ shift was slightly higher, resulting in a shift by 82.74 ± 10.17
252 mV. This is consistent with previous studies, as BKα channel gating is primarily voltage-driven
253 at very low Ca_i^{2+} concentrations and Ca_i^{2+} driven at high concentrations, while in the low-
254 micromolar range (i.e., around 1 μM), Ca_i^{2+} binding sites are partially occupied, resulting in
255 nonlinear gating where enhanced modulator effects can occur (Cui, Cox and Aldrich, 1997;
256 Magleby, 2003; Clay, 2017).

257

258 *α-Mangostin activation mechanism on single-channel and macroscopic current level*

259 The marked slowing of deactivation visible as the slow tail current decay in macroscopic
260 current recordings suggests that individual channels are open for longer periods of time in the
261 presence of α-Mangostin. To investigate the effect of α-Mangostin on individual channels, we
262 recorded single channel currents in excised inside-out patches from HEK293 cells in the
263 presence of 100 nM free Ca_i^{2+} (Fig. 3A). Under these conditions, the open probability (P_o) of
264 BK channels at a potential of +40 mV was very low (0.002 ± 0.0008), but rose to 0.77 ± 0.08
265 after activation by 10 μM α-Mangostin (Fig. 3B) with only very brief closings (Fig 3A, 1s inset).
266 The single channel amplitude derived from the all-points-histogram was not different between
267 basal and α-Mangostin activated states (9.18 ± 0.29 pA and 9.76 ± 0.26 pA; Fig. 3B). We

constructed dwell time distributions to determine the differences in the duration that a single channel resides in the closed or open state (Fig. 3C). The Log closed dwell time distributions showed a large shift of the main component to shorter dwell times, from 2.38 ± 0.23 (237 ms) to -1.39 ± 0.36 (less than 0.1 ms). The open dwell time distribution revealed that the log open time was markedly reduced from -0.84 ± 0.45 to 0.8 ± 0.24 (i.e. from 0.14 ms to 6.28 ms). The fact that the open and closed times were both affected suggests that α-Mangostin can bind to the open and the closed state. Accordingly, application of α-Mangostin on closed BK-channels (at – 80mV) resulted in maximal activation with the first depolarization pulse, indicating that α-Mangostin reached its site of action during the closed period (Fig. 3D).

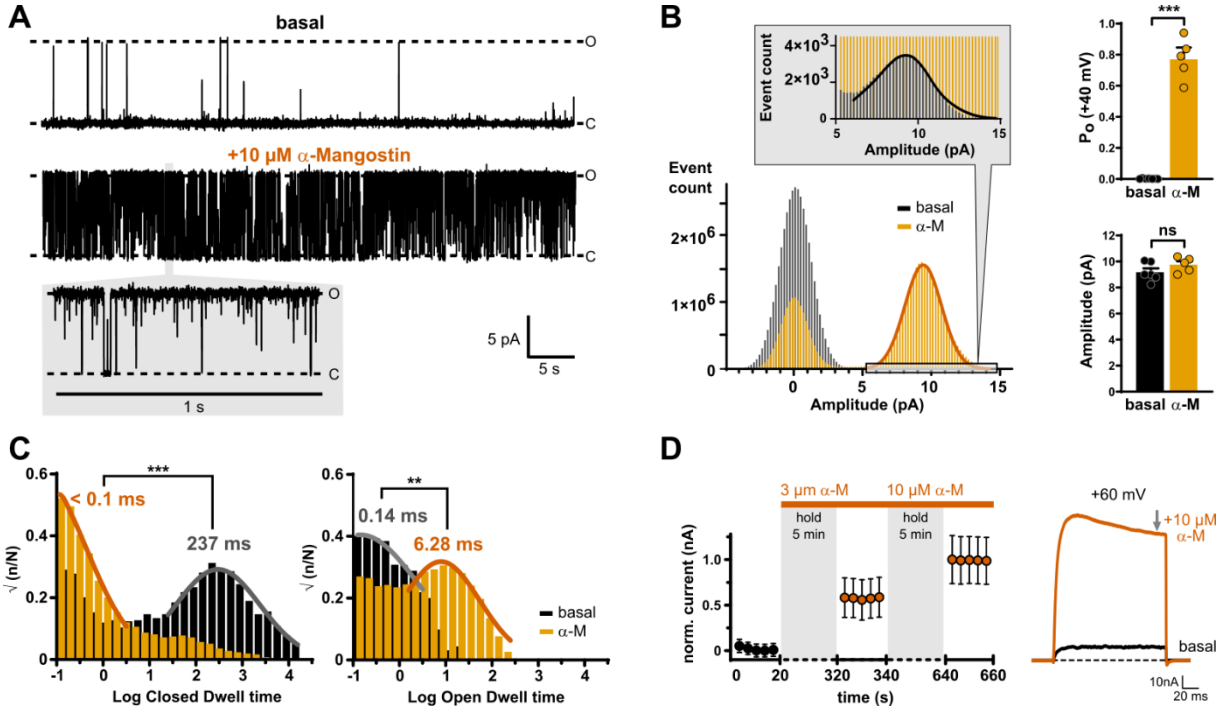

Figure 3: Activation mechanism of α-Mangostin. (A) Exemplary current traces of a single BKα channel in the basal state and after activation by 10 µM α-Mangostin (1 min recordings; inset shows 1 s; O and C denote open and closed levels). Single-channel currents were recorded at +40 mV in inside-out patches from transiently transfected HEK293 cells in symmetrical potassium gradients with 100 mM free Ca_i^{2+} (n=4-7). **(B)** All-points histograms with Gaussian fits for the basal and α-Mangostin activated state, and bar graphs of the derived mean ± SEM open probabilities (P_o) and amplitudes. The inset magnifies the open peak in the basal state. **(C)** Closed and open dwell time histograms with fits for channels in the basal and in the α-Mangostin activated state derived after event detection in single-channel measurements as shown in (A). **(D)** Normalized mean ± SEM currents of BKα channels before and after application of 3 µM or 10 µM α-Mangostin in the closed state. Channels were held closed at -80 mV and only very shortly pulsed to +60 mV after 5 min incubation to assess the current size/activation state of the first and the following pulses. Measurements were done in transiently transfected HEK293 cells in whole-cell mode in physiological potassium gradients with 100 nM Ca_i^{2+} as shown by the representative current traces to the right and steady-state currents were analyzed (grey arrow). Data and statistics see Table S6.

293 *Localization of the α-Mangostin binding site*

294 We recently described the polypharmacology of the class of negatively charged activators
295 (NCA) in different potassium channels, specifically in TREK-1 and BK channels. The BK
296 channel opener GoSlo-SR-5-6 also activated TREK-1 channels, while BL-1249 known as
297 TREK/TRAAK channel opener, also activated BK channels. We identified their common
298 binding site in the pore close to the fenestration of TREK-1 channels and Molecular Dynamics
299 (MD) simulations predicted the equivalent binding site in the pore of BK channels (Schewe *et*
300 *al.*, 2019). The question arose if α-Mangostin could also occupy this binding site, as in part
301 suggested in a docking by (Kim *et al.*, 2023), who proposed that P183 and L304, which both
302 are part of the NCA binding site, interact with α-Mangostin in TREK-1 channels. Therefore, we
303 measured the dose-dependent α-Mangostin activation of TREK-1 wildtype channels and its
304 'signature' mutant of the fenestration, L304C. As expected, the apparent affinity is markedly
305 reduced in the L304C mutant in the measurable concentration range (Fig. S2A). Quaternary
306 ammonium ions are known to occupy the central cavity of K^+ channels as TREK-1 and BK just
307 below the SF near the NCA binding site (Li and Aldrich, 2004; Piechotta *et al.*, 2011; Fan *et*
308 *al.*, 2023). In a competition experiment, we recorded dose-response relationships and
309 determined theIC_{50} value for Tetrapentylammonium (TPA) with and without preactivation by 10
310 μM α-Mangostin. The TPA IC_{50} value increased ≈9-fold from 0.72 ± 0.64 μM to 6.33 ± 0.86 μM
311 in the presence of α-Mangostin (Fig. S2B), showing that α-Mangostin was present in the pore
312 and hindered the access of TPA to its binding site. Finally, cysteine scanning mutagenesis of
313 residues in M2 and M4 revealed that mainly G181, I182, P182 on M2 and G308 in M4 were
314 involved, while most M4 residues tested had intermediary effects (Fig. S2C), suggesting that
315 the binding region of α-Mangostin between M2 and M4 overlaps with the NCA binding site
316 identified with the help of BL-1249, but is not completely identical (Fig. S2D).

317 We next probed if α-Mangostin accesses the pore cavity of BKα channels, as in TREK
318 channels, or binds elsewhere in the protein. We conducted a competition experiment as above
319 and measured the dose-dependent inhibition by 0.1, 1 and 10 μM Tetrahexylammonium
320 (THexA; Fig. 4A). In the presence of α-Mangostin, the inhibition by THexA was clearly reduced,
321 and the apparent THexA affinity (as estimated IC_{50}) was steeply decreased ≈21-fold from 77.51
322 ± 5.53 nM to 1.64 ± 0.58 μM, showing that the presence of α-Mangostin hindered the access
323 of THexA to its binding site. This is consistent with previous findings that GoSlo-RS-5-6, which
324 binds in the BK pore, also competes with THexA (Roy *et al.*, 2012; Webb *et al.*, 2015; Schewe
325 *et al.*, 2019). In contrast, the presence of BC5, an activator shown to bind at the interface
326 between the transmembrane and intracellular domains (Zhang *et al.*, 2022), did not interfere
327 with THexA binding (estimated THexA IC_{50} 45.60 ± 8.05 nM; Fig. 4A).

328 At least one hydroxyl group of α-Mangostin is predicted to be negatively charged in
329 physiological pH (National Center for Biotechnology Information, 2025), therefore we tested
330 the impact of solution pH on the activation potency. Indeed, the shift in $V_{½}$ induced by 10 µM
331 α-Mangostin was pH-dependent (Fig. 4C). In pH 6, the shift was reduced to 34.71 ± 5.63 mV,
332 while it increased to 75.97 ± 2.02 mV in pH 8.5, indicating that the negative charge is critical
333 for effective activation and α-Mangostin might resemble an NCA-like compound.

334 In addition, we used molecular docking to determine the location of a possible binding site in
335 the BKα inner pore. We obtained 20 poses which were all located at the cavity wall in middle
336 S6 between residues I308 and V319, in a pocket below the SF, without obstructing the central
337 passageway for K^+ ions (Fig. S3). Three poses were clustered with a binding energy of -8.58
338 kcal mol^{-1}, where the hydrophobic core was wedged in between S6 and S6 of the adjacent
339 subunit. For the best pose, possible molecular interactions were predicted for the residues
340 I308, L312, F315 and A316 in S6 (Fig. 4B; Fig. S3).

341 To functionally investigate the predicted binding site, we mutated residues in the pore-lining
342 S6 helix with side chains facing into the cavity. Many substitutions in this region affect gating
343 of BK channels and are involved in intersubunit S6-S6 contact (Wu *et al.*, 2009; Zhou, Xia and
344 Lingle, 2011). Therefore, we chose only substitutions that were most WT-like with respect to
345 Ca_i^{2+} and voltage sensitivity, i.e., I308A, L312M, A316P for the hits from the docking, and
346 additionally S317R and Y318S as internal controls that were not predicted to be part of the
347 binding site (Chen, Seebohm and Sanguinetti, 2002; Chen, Yan and Aldrich, 2014). We first
348 assessed the shift in voltage activation induced by 10 µM α-Mangostin (Fig. 4D, E). $V_{1/2}$ shifts
349 of Y318S and S317R were not or only moderately different compared to the wildtype channel
350 (41.46 ± 5.17 mV and 34.33 ± 3.37 mV). In contrast, the three mutants I308A, L312M, and in
351 particular A316P had a markedly reduced shift in $V_{1/2}$ (19.97 ± 3.12 mV, 27.89 ± 5.42 mV, and
352 4.56 ± 1.23 mV, respectively). To ensure that the almost absent shift in A316P was not caused
353 by a general disruption of allosteric signal transduction, we also included A316G, which
354 showed a reduction in $V_{1/2}$ comparable to I308A and L312M (23.57 ± 2.05 mV).

355 Furthermore, we tested GoSlo-SR-5-6 as alternative activator, which was shown to bind in the
356 same pore region involving A316 (Webb *et al.*, 2015; Schewe *et al.*, 2019; Zhang *et al.*, 2022).
357 Like for α-Mangostin, I308A and A316P reduced the shift in $V_{½}$ induced by 1 µM GoSlo-SR-5-
358 6 from 42.71 ± 3.05 mV to 25.89 ± 4.05 and 25.0 ± 2.8 mV; however, A316P did not abolish
359 GoSlo-SR-5-6 activation, showing that the complete loss of activation for α-Mangostin was
360 likely caused primarily by a loss of binding and not by an inference of the mutation with the
361 drug transduction mechanism (Fig. 4F). Hence, we conclude that α-Mangostin binds to and
362 activates BKα channels via the upper S6 segment, critically involving residues I308, L312, and
363 A316.

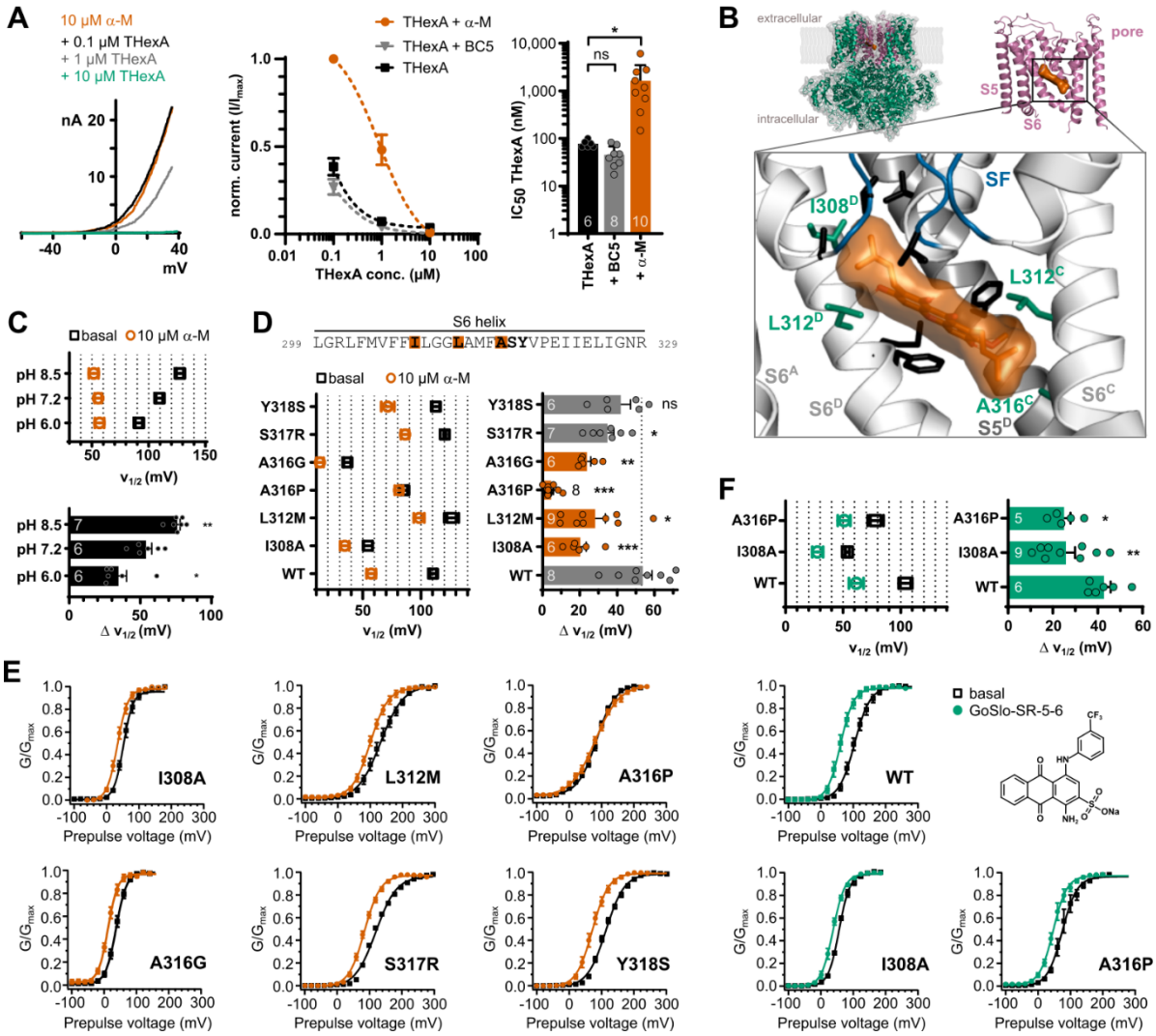

Figure 4: Investigation of the binding site of α-Mangostin in BKα channels. (A) Competition experiment showing a reduction of the block caused by THexA in the presence of α-Mangostin. Left, representative current traces for different THexA concentrations in the presence of 10 µM α-Mangostin; middle, competition experiment analysis showing the relative current of BKα channels in different THexA concentrations in the absence and in the presence of 10 µM α-Mangostin or 100 µM BC5, which does not bind in the pore; and right, estimated IC_{50} values of THexA alone and in the presence of α-Mangostin or BC5. Whole-cell currents were recorded from transiently transfected HEK293 cells with a ramp protocol (-100 mV to +50 mV) in a physiological potassium gradient with 100 nM free Ca_i^{2+} and data are shown as mean ± SEM at +40 mV. **(B)** Molecular docking of α-Mangostin to the human BK channel structure (PDB ID 6v3g). The full-length structure (green) was reduced to the inner pore region (pink) for the docking, and the zoom-in shows the best pose for α-Mangostin with interacting residues in stick representation; green residues mark hits from the following functional assay. Protein chain B was removed for clarity. **(C)** Voltage of half-maximal activation ($V_{½}$) before and after activation by 10 µM α-Mangostin in different pH and the resulting shifts in $V_{½}$ (Δ $V_{½}$). The pH was changed intra- and extracellularly. **(D)** Voltage of half-maximal activation ($V_{½}$) before and after activation by 10 µM α-Mangostin, and the resulting shifts in $V_{½}$ (Δ $V_{½}$). **(E)** GV-relationships for the six BKα mutants in the S6 segment. **(F)** Voltage of half-maximal activation ($V_{½}$) before and after activation by 1 µM GoSlo-SR-5-6, the resulting shifts in $V_{½}$ (Δ $V_{½}$), and the GV-relationships for the wildtype and

two BKα mutants. GV-relationships were measured as in Fig. 2, and all data represent mean ± SEM. Data and statistics see Tables S9 – S12.

α-Mangostin activation in BK-Ca_v nanodomains

In resting smooth muscle cells, there is no BK channel activation within their physiological voltage range. However, in native tissue, BK channels are organized in nanodomains together with Ca_v channels that can generate an increase in Ca_i^{2+} concentration in the range of several orders of magnitude in their vicinity, allowing BK channels to open (Shah, Guan and Yan, 2022). This BK-Ca_v complex can be restored in heterologous expression systems, and, as the intracellular solution contains 5 mM EGTA to suppress an overall increase of Ca_i^{2+}, BK channels will activate only when nearby Ca_v channels cause a high local Ca_i^{2+} concentration (Berkefeld *et al.*, 2006; Berkefeld and Fakler, 2008). BKα/β1 channels expressed alone therefore produced virtually no current upon stepwise depolarization to +50 mV (Fig. 5A, B), but could be activated by α-Mangostin (Fig. 5A, B). In BKα/β1-Ca_v complexes, Ca^{2+} inward currents were elicited, which allowed BKα/β1 channels to open in a more negative voltage range, and these BKα/β1 currents were further enhanced by 10 µM α-Mangostin (Fig. 5A, B). The α-Mangostin-activated current through BKα/β1 channels in the Ca_v complexes (as difference between BKα/β1-Ca_v currents before and after activation) was activated at more negative potentials than in BKα/β1 channels alone (Fig. 5B). Hence, α-Mangostin could potentiate BKα/β1 channel currents upon local Ca_i^{2+} increase through nearby Ca_v-channels, as it could occur upon a Ca_i^{2+} spike in a cell.

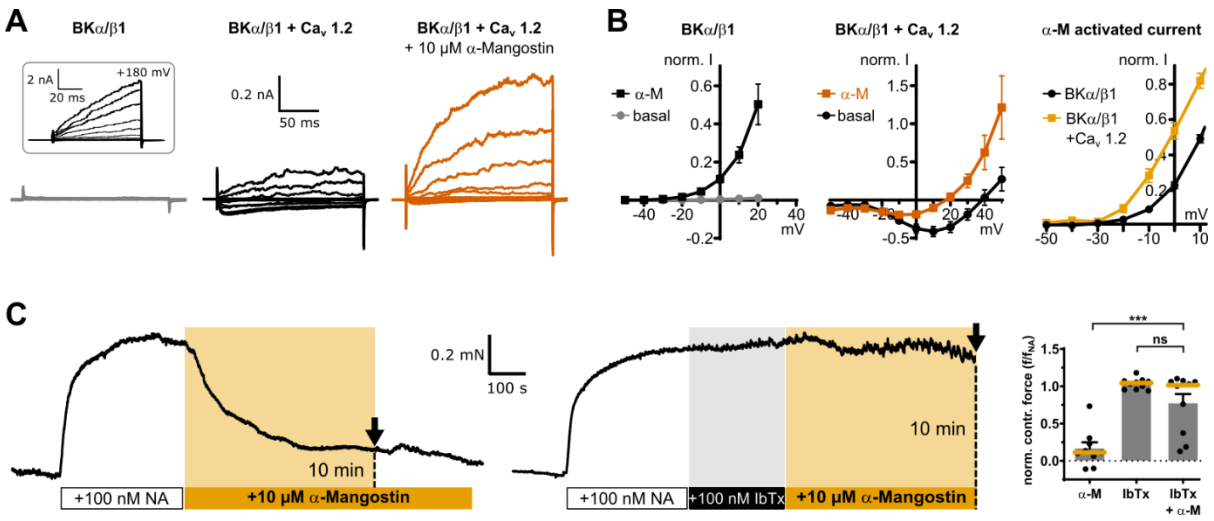

Figure 5: α-Mangostin activation of BK channels in physiological settings. (A) Representative whole-cell current traces of BKα/β1 channels alone and BKα/β1 coexpressed with $Ca_v1.2$ channels before and after application of 10 µM α-Mangostin. Currents were measured in Ca_i^{2+}-free conditions in a physiological potassium gradient with

408 a family of voltage steps from -50 mV to +50 mV in 10 mV increments. The inset shows voltage activation with a
409 family protocol up to +200 mV to show the presence of BKα/β1 channels. **(B)** Currents of BKα/β1 channels and
410 BKα/β1 – Ca_v complexes before and after application of 10 µM α-Mangostin plotted against voltage. The last panel
411 shows the α-Mangostin-activated currents for the range -50 to 10 mV obtained by subtracting the current before α-
412 Mangostin application from the current after application for each potential (mean ± SEM, n=8-11 for each condition).
413 **(C)** Representative contraction force recordings of aortic preparations from mice. 10 µM α-Mangostin were either
414 applied directly to aortic preparations precontracted with 100 nM Noradrenaline (NA; top), or the precontracted
415 preparations were incubated with 100 nM Iberiotoxin (IbTx) before α-Mangostin application and the contraction
416 force was analyzed 10 min after α-Mangostin addition (dotted lines in recordings). The bar graph shows the
417 normalized contraction force of preparations as mean ± SEM together with the median (orange). Data and statistics
418 see Table S13.

419

420 *α-Mangostin relaxes vascular tissue in aortic preparations via BK channels*

421 Cardiovascular benefits of Mangostins could arise from vasodilatory effects leading to a
422 reduction of blood pressure. Years ago, a study reported that γ-Mangostin, in which the
423 methoxy group of α-Mangostin is exchanged for a hydroxyl group, induced relaxation of rat
424 aortic rings, but no molecular target was found (Tep-Areenan and Suksamrarn, 2012). We
425 sought to demonstrate that Mangostin-induced vasorelaxation of native vascular tissue is
426 indeed mediated by BK channels. Aortic preparations from mice were equilibrated at a
427 contraction force of 2-3 mN and subsequently precontracted half-maximally with 100 nM
428 noradrenaline. The application of 10 µM α-Mangostin quickly and efficiently induced relaxation,
429 while relaxation was absent or greatly attenuated when the specific BK channel inhibitor
430 Iberiotoxin (IbTx) was applied for 5-6 minutes before α-Mangostin was administered (Fig. 5C).
431 In total, α-Mangostin reduced the normalized contraction force of the preparations by more
432 than 85 % (to 0.16 ± 0.08) compared to the precontracted state, while it did not change after
433 IbTx application alone (1.04 ± 0.002) or after preblock of BK channels (0.78 ± 0.12), proving
434 that BK channels must mediate the vasodilative effect seen upon Mangostin treatment.

435

436 **Discussion**

437 We provide mechanistic insight into how a natural xanthone compound modulates BK
438 channels, which are major players in vascular function. α-Mangostin activates BK channels by
439 shifting their voltage sensitivity and slowing deactivation, with lesser effects on activation and
440 marked effects on Ca_i^{2+} sensitivity. We show that binding of α-Mangostin is state-independent,
441 and we provide evidence for a binding site in the gating-sensitive S6 segment.

442 *Mangostin binds to closed and open channels and promotes the open state*

443 BK channel P_o is controlled by Ca_i^{2+}, voltage, a shift of the closed-open equilibrium of the pore
444 domain, or a combination of those stimuli (Cui, Cox and Aldrich, 1997). Mangostin shifted the
445 voltage activation curve to more negative potentials, meaning an increased open probability at
446 negative voltages. The slope of the GV-relationship was not changed neither in homomeric
447 BKα nor in the smooth muscle BKα/β1 channels, indicating that voltage sensitivity itself was
448 not directly affected by α-Mangostin. Shifts in the $V_{½}$ values induced by α-Mangostin were
449 present over a wide range of Ca_i^{2+} concentrations (0.1, 1 and 10 μM), which implies that the
450 closed-open equilibrium is shifted towards the open state by a mechanism distinct from Ca_i^{2+}
451 sensing, or that at least the Ca_i^{2+} sensing mechanism is not likely to contribute significantly to
452 α-Mangostin activation. The higher shift observed in in 1 μM Ca_i^{2+} likely reflects the known non-
453 linear gating features that result from pronounced allosteric coupling of voltage and Ca_i^{2+}
454 signals in this concentration range (Cui, Cox and Aldrich, 1997; Magleby, 2003; Clay, 2017;
455 Sun and Horrigan, 2022).

456 The activation can be mainly explained by the marked slowing of the deactivation time
457 constants. Consistently, the mean open dwell time was increased in the single channel
458 measurements, while we observed no change in amplitude with and without α-Mangostin
459 (corresponding to a conductance of ≈240 pS). The impact on open as well as closed dwell time
460 distributions and the instantaneous activation of macroscopic currents from the closed state
461 suggest that the molecule binds state-independently.

462 In the presence of the β1 subunit, which is present in vascular BK channels (Knaus *et al.*,
463 1994), the activation characteristics were enhanced. The activation time course was little
464 affected in BKα channels, but in BKα/β1 channels an acceleration of the activation caused by
465 α-Mangostin became more prominent, counteracting the slow activation kinetics brought by
466 the β1 subunit (McManus *et al.*, 1995). Additionally, the slow deactivation time course in the
467 presence of the β1 subunit was further slowed down remarkably. As the affinity (as estimated
468 EC_{50}) was very similar and the binding site is located in the S6 segment in the inner pore, the
469 stronger shift in the $V_{½}$ value is likely not due to changes in binding, but caused by an enhanced
470 shift of the closed-open equilibrium toward the open state, such as the stabilization of the
471 voltage sensor in an active conformation. Such β-subunit dependent effects have also been
472 reported for other modulators, e.g., DHS-I (McManus *et al.*, 1993; Giangiacomo *et al.*, 1998),
473 DHA (Hoshi, Tian, *et al.*, 2013), arachidonic acid (Martín *et al.*, 2021),17β-Estradiol (Valverde
474 *et al.*, 1999), and some GoSlo compounds (Large *et al.*, 2015).

475 *The binding site of α-Mangostin includes residues in the gating-sensitive S6 segment*

476 We demonstrated the presence of α-Mangostin in the channel pore by competition for binding
477 with quaternary ammonium ions known to bind below the SF (Li and Aldrich, 2004; Fan *et al.*,

478 2023), and, predicted by molecular docking, identified residues in the S6 segment that are part
479 of the binding site.

480 α-Mangostin binds in the cleft formed by the S6 helices of adjacent subunits, and substitution
481 of the nonpolar residues I308, L312, and especially A316 most strongly reduced the shift in $V_{½}$
482 induced by α-Mangostin. All residues are known to participate in gating: they are part of a
483 hydrophobic network within S6 that acts as hinge upon channel opening, and polar
484 substitutions strongly favor the open state (Zhou, Xia and Lingle, 2011; Chen, Yan and Aldrich,
485 2014; Hite, Tao and MacKinnon, 2017). L312 has further been shown to stabilize intersubunit
486 interaction with F315, whose destruction opens the channel (Wu *et al.*, 2009).

487 The α-Mangostin binding region overlaps with the reported binding site of the NCA GoSlo-SR-
488 5-6, where L312, A316, S317 and V319 are involved (Webb *et al.*, 2015; Schewe *et al.*, 2019),
489 but it is not identical. When we functionally investigated the α-Mangostin binding site close to
490 the fenestration in TREK-1 channels, we also found only a partial overlap with key residues
491 involved in the NCA binding site. Interaction with P183 and L304 was consistent with an earlier
492 molecular docking (Kim *et al.*, 2023), but the strongest reduction of activation was found for
493 residues in M2 rather than M4.

494 *Mechanism of Mangostin activation*

495 We expect that small structural or electrostatic changes in this gating-sensitive region strongly
496 affect the closed–open equilibrium (Wu *et al.*, 2009; Zhou, Xia and Lingle, 2011; Chen, Yan
497 and Aldrich, 2014). Previous studies suggest several alternative mechanisms by which α-
498 Mangostin could induce channel opening. We have shown that NCAs bind to a region below
499 the selectivity filter (SF) in several K^+ channels, such as K_{2P} (e.g., TREK), hERG, or BK
500 channels to induce channel opening (Schewe *et al.*, 2019). We speculated that the negative
501 charge common to these activators might alter SF ion occupancy via an electrostatic
502 mechanism, thereby promoting SF opening. Our finding that the potency of α-Mangostin
503 depends on pH suggests that a negative charge may also be critical for its activation
504 mechanism. However, the importance of the SF for BK gating remains unresolved.
505 Furthermore, α-Mangostin also did not increase the single-channel conductance as seen for
506 NCAs in TREK-2 channels, which are known to be gated at the SF (Schewe *et al.*, 2019).
507 Therefore, the contribution of the SF to the Mangostin effect requires further investigation.
508 Alternatively, α-Mangostin binding to the gating-critical S6 region could induce gating at a
509 putative lower gate; however, such a gate is currently speculative, as the available BK
510 structures lack clear evidence for a lower gate (but the final closed state may still be elusive)
511 (Hite, Tao and MacKinnon, 2017; Tao, Hite and MacKinnon, 2017).

512 In addition to the concepts of an SF gate or a lower gate, hydrophobic gating has been
513 proposed as an alternative gating mechanism in BK channels. MD simulations suggest that
514 the pore of metal-free (presumably closed) BK structures undergoes dewetting, whereas the
515 pore of metal-bound (presumably open) structures remains hydrated (Jia *et al.*, 2018; Gu and
516 de Groot, 2023). Thus, binding of negatively charged α-Mangostin might prevent or antagonize
517 dewetting of the hydrophobic cavity and thereby stabilize the conductive pore state. Indeed, a
518 recent MD study suggested that the NCA NS11021, a smooth muscle relaxant with a
519 biarylthiourea structure, can enter the dewetted BK pore to promote hydration (Rockman,
520 Vouga and Rothberg, 2020b; Nordquist, Jia and Chen, 2024). However, the same MD
521 simulations also indicated that NS11021 has no stable binding pose but engages in various
522 hydrophobic interactions with pore-cavity residues. In contrast, our results suggest a more
523 stable binding pose with specific interactions, as inferred from our mutagenesis data. Clearly,
524 further work is required to elucidate the mechanism of BK channel gating and the exact way
525 Mangostin and other NCAs modulate this process to promote channel activation.

526 *Activation of BK channels in nanodomains and relaxation of aortic tissue*

527 Our data demonstrate that Mangostin is able to potentiate Ca_v-induced BK currents, and that
528 Mangostin-activated BK channels are responsible for relaxation of mouse vascular tissue,
529 explaining the reduction of blood pressure reported in a recent animal study (Xu *et al.*, 2024).

530 We reconstructed nanodomains of BK and $Ca_v1.2$ channels, as e.g. present in arterioles
531 (Berkefeld *et al.*, 2006; Tykocki, Boerman and Jackson, 2017). In smooth muscle cells, BK
532 activation is strictly coupled to changes in Ca_i^{2+}. Physiological Ca_i^{2+} concentrations lie between
533 100 nM in the resting state, 0.4-1 µM upon activation of a Ca^{2+} mobilizing receptor (Savineau
534 and Marthan, 2000; Hill-Eubanks *et al.*, 2011), and up to several ten micromolar (10-40 µM)
535 when sparks form locally (ZhuGe *et al.*, 2002; Berkefeld, Fakler and Schulte, 2010). Transient
536 outward currents through activated BK channels then act as negative feedback, repolarize the
537 cell and terminate Ca^{2+} influx (Shah, Guan and Yan, 2022). We demonstrated that the α-
538 Mangostin activated current is potentiated by the coupling to Ca_v channels. BKα/β1 currents in
539 in the physiological voltage range of smooth muscle cells (-50 - -30 mV) would be very small
540 in resting Ca_i^{2+}, while the P_o would be already very high when exceeding 10 µM Ca^{2+}, leaving
541 less room for activation. α-Mangostin would particularly impact potentiation of BK currents
542 upon physiological Ca^{2+} elevation (i.e. between 1 and 10 µM) and would synergistically lower
543 the BKα/β1 activation threshold to enhance the negative feedback mechanism.

544 Accordingly, our investigation of precontracted aortic tissue from mice showed a remarkable
545 and robust relaxation after application of α-Mangostin. Such relaxation of aortic rings after
546 application of α- or γ-Mangostin were reported before (Chairungsrilerd *et al.*, 1996, 1997; Tep-
547 Areenan and Suksamrarn, 2012) but the exact molecular target remained inconsistent. Given

548 the strong activation of BK channels and as the relaxation was absent upon preincubation with
549 the selective inhibitor IbTx in our experiments, BK channels must represent the molecular
550 target of Mangostins in vascular smooth muscle cells.

551 Interestingly, relaxation was also reported for other xanthone derivatives (Cheng and Kang,
552 1997; Wang *et al.*, 2002; Capettini *et al.*, 2009; Câmara *et al.*, 2010; Diniz *et al.*, 2013), which
553 legitimates further research of substituted xanthones as pharmacophore. Robust data of
554 bioavailability and the existence and nature of active metabolites are currently lacking. A small
555 study claimed that α-Mangostin was bioavailable in humans after supplement ingestion (Kondo
556 *et al.*, 2009). Animal research analyzed metabolites and showed that maximal plasma
557 concentrations are reached 1 hour after oral intake in mice (Ramaiya *et al.*, 2012; Petiwala *et*
558 *al.*, 2014; Han *et al.*, 2015). However, no metabolites have been functionally investigated to
559 help in optimization of the Mangostin pharmacophore; however, our finding that γ-Mangostin
560 has a slightly higher potency in activating TREK-1 and BKα channels may be a starting point.

561 Our screen across different K^+ channel families revealed that other representatives of the K_{2P}
562 (TWIK-1 and TASK-3) were particularly inhibited by more than 60 %. This could also link other
563 claimed benefits of Mangostin to their molecular targets. Importantly, hERG currents were
564 unaffected, mitigating the cardiotoxicity risk upon consumption of Mangostin nutraceuticals.
565 BK channel function is decreased in chronic conditions that are often associated with the lack
566 of a balanced diet and age, such as metabolic syndrome, diabetes, and obesity (Tykocki,
567 Boerman and Jackson, 2017). Consequences as increased vascular tone and hypertension,
568 ultimately leading to reduced cardiovascular health and premature death, may therefore be
569 addressed with Mangostin xanthones as a potential new class of BK channel activators.

570

571

572 **Methods and Materials**

573 *Substances*

574 α-Mangostin, γ-Mangostin, TPA, THexA, MgATP, NaGTP and noradrenaline were purchased
575 from Merck (Darmstadt, Germany). BC5 (Arg-4-methoxy-2-naphthylamine) was obtained from
576 MP Biomedicals (Irvine, USA), and Iberiotoxin from Alomone Labs (Jerusalem, Israel). GoSlo-
577 SR-5-6 (sodium 1-amino-4-((3trifluoromethylphenyl)amino)-9,10-dioxo-9,10-
578 dihydroanthracene-2-sulfonate)) was provided by Mark Hollywood. Mangostane food
579 supplement stating a content of 50 mg α-Mangostin per capsule was ordered online
580 (Swanson.com). Aiming for a 10 mM stock solution with respect to α-Mangostin, 205 mg of the
581 powder found in the capsules was dispersed in 5 ml DMSO, brought into solution by vortexing
582 and ultrasonication, and filtered through a 0.45 µM PTFE membrane to remove remaining
583 particulate matter. TPA, THexA, NA, BC5, and Iberiotoxin were prepared as 1:1000 stocks in
584 H_2O, and the Mangostins and GoSlo-RS-5-6 in DMSO at 50 mM. Aliquots were stored at -
585 20°C and diluted to the final concentration in extracellular solution.

586 *Molecular biology, cell culture and transfection*

587 Coding sequences for channels and subunits listed in Table 1 were subcloned in pFAW or
588 pcDNA3.1 vectors containing a CMV promotor for expression in HEK293 cells. Amino acid
589 substitutions were introduced by site-directed mutagenesis PCR according to the QuikChange
590 protocol (Stratagene, La Jolla, USA) with custom primers containing the desired base
591 exchange. All constructs were verified by Sanger sequencing. To enhance plasma membrane
592 expression, the retrieval motif was removed in hTWIK-1 and hTWIK-2 channels by the
593 substitutions I293A, I294A (Feliciangeli *et al.*, 2010) and I289A, L290A (Bobak *et al.*, 2017),
594 respectively, yielding hTWIK-1^m and hTWIK-2^m channels.

595 *Table 1: Channels and subunits used in this study*

Name	Organism	Gene name	Genbank Acc. No.
hTREK-1b	*Homo sapiens*	KCNK2	NM_001017425.2
hTALK-1	*Homo sapiens*	KCNK16	NM_032115.3
hTRESK	*Homo sapiens*	KCNK18	NM_181840.1
hTWIK-1^m	*Homo sapiens*	KCNK1	NM_002245.3
hTWIK-2^m	*Homo sapiens*	KCNK6	NM_004823.1
hTASK-3	*Homo sapiens*	KCNK9	NM_001282534.1
hTHIK-1	*Homo sapiens*	KCNK13	NM_022054.3
mBKα (Slo1.1)[1]	*Mus musculus*	Kcnma1	NM_001014797.3
mβ1	*Mus musculus*	Kcnmb1	NM_031169.4
hK_v 1.1	*Homo sapiens*	KCNA1	NM_000217.3

hK_v 1.3	*Homo sapiens*	KCNA3	NM_002232.5
hK_v 11.1 (hERG1b)	*Homo sapiens*	KCNH2	AJ512214.1
hK_{ir} 1.1 (ROMK)	*Homo sapiens*	KCNJ1	NM_000220.4
mK_{ir} 2.1	*Mus musculus*	KCNJ2	NM_008425.4
Ca_v 1.2:			
$Ca_v\alpha$ 1C	*Rattus norvegicus*	Cacna1c	M67515.1
Ca_v β1	*Rattus norvegicus*	Cacnb1	NM_017346.1
Ca_v α2δ1	*Rattus norvegicus*	Cacna2d1	AF286488

596 [1] G/S-rich N-terminus removed, corresponding to residues 65-1236 of the native channel

597 HEK293 cells were cultivated in Dulbecco's Modified Eagles Medium (DMEM) supplemented
598 with 10 % FCS and penicillin/streptomycin (100 U ml^{-1}/100 µg ml^{-1}) in 5 % CO_2 at 37 °C. For
599 cultivation of CHO-K1 cells, the medium was additionally supplemented with non-essential
600 amino acid mix (Gibco MEM-NEAA; Thermo Fisher, Schwerte, Germany) and 10 mM Hepes.

601 HEK293 cells were transiently transfected with Lipofectamine 2000 (Invitrogen, Thermo Fisher,
602 Schwerte, Germany) or FuGENE (Promega, Walldorf, Germany) as to the manufacturer's
603 instructions and incubated overnight. pEYFP was included as transfection marker. In BKα/β1
604 coexpressions, the β1 subunit was used in 10-fold excess to ensure a uniform channel
605 population. Cells were trypsinized and seeded onto glass coverslips 2-3 h prior to
606 electrophysiological experiments.

607 *Electrophysiology*

608 Voltage clamp experiments were conducted with a HEKA EPC10 amplifier controlled by
609 Patchmaster Software (v2.78; HEKA Elektronik, Lambrecht, Germany). Standard
610 measurements were done in transiently transfected HEK293 cells in the whole-cell
611 configuration in physiological potassium gradients. Pipettes were pulled from thin-walled
612 borosilicate glass, fire-polished, and had resistances of 1.4 – 2 MΩ. Series resistance was
613 compensated to at least 70 %. The extracellular solution contained (in mM): 135 NaCl, 5 KCl,
614 2 $CaCl_2$, 2 $MgCl_2$, 10 D(+)-glucose, 10 Hepes (pH 7.3). The intracellular solution was (in mM):
615 140 KCl, 2 $MgCl_2$, 1 $CaCl_2$, 2.5 EGTA, 10 Hepes (pH 7.3), corresponding to ≈100 nM free Ca^{2+}.
616 For K_{ir} 1.1 and 2.1 channel recordings, 3 mM MgATP and 0.3 mM NaGTP were included.
617 Where indicated, K^+ was substituted for Cs^+ to reduce the outward currents of BK channels.
618 Cells were held at -80 mV and a voltage ramp from -100 mV to +60 mV of 1 s duration was
619 applied every 5 s. For K_v channels a rectangle pulse was used as indicated in the figure
620 legends.

621 The activation of BK channels was measured as conductance G in symmetrical potassium
622 solutions to ensure a unitary conductance across the voltage range. Cs^+ was used as

623 intracellular ion to reduce outward currents. The extracellular solution contained (in mM): 140
624 KCl, 2 $CaCl_2$, 2 $MgCl_2$, 10 D(+)-glucose, 10 Hepes (pH 7.3). The intracellular solution was (in
625 mM): 140 CsCl, 2 $MgCl_2$, 1 $CaCl_2$, 2.5 EGTA, 10 Hepes (pH 7.3), corresponding to ≈100 nM
626 free Ca^{2+} (calculated with WEBMAXC
627 (https://somapp.ucdmc.ucdavis.edu/pharmacology/bers/maxchelator/webmaxc/webmaxcS.ht
628 m). For recordings with 1 µM and 10 µM free Ca_i^{2+}, $CaCl_2$ and EGTA were raised to 2 mM /
629 2.2 mM and 2 mM / 4.04 mM, respectively. Cells were held at negative holding potentials and
630 currents were elicited with a family of rectangle voltage pulses in 20 mV increments to positive
631 potentials as needed for saturation of the tail currents, followed by a repolarization step to elicit
632 the tail currents as detailed in the figure legends. The currents were analyzed with Fitmaster
633 (HEKA Elektronik, Lambrecht, Germany), and conductance-voltage (G-V) relationships were
634 generated from normalized tail currents and fit to a standard Boltzmann relationship (1) to
635 obtain $V_{1/2}$ values. Individual fits were then averaged for mean $V_{1/2}$ values.

636
$$\frac{G}{G_{max}} = \frac{1}{1 + e^{\frac{(V - V_{1/2})}{k}}}$$

637 where G_{max} is the maximal tail current, $V_{1/2}$ is the voltage of half-maximal activation of the
638 current, and k is the slope factor.

639 Activation in different pH was measured using the following solutions: Extracellular solution pH
640 8.5 contained (in mM): 140 KCl, 2 $CaCl_2$, 2 $MgCl_2$, 10 D(+)-glucose, 10 Ampso; intracellular
641 solution pH 8.5 contained (in mM): 140 $CsCl_2$, 10 Ampso, 2 $MgCl_2$, 1 $CaCl_2$, 2.05 EGTA.
642 Extracellular solution pH 6 was (in mM): 140 KCl, 2 $CaCl_2$, 2 $MgCl_2$, 10 D(+)-glucose, 10 MES;
643 intracellular solution pH 6 contained (in mM): 140 $CsCl_2$, 10 MES, 2 $MgCl_2$, 0.5 $CaCl_2$, 11
644 EDTA. The pH was changed intra- and extracellularly.

645 In TPA competition experiments for TREK-1 channels a dose-response relationship in the
646 absence and presence of α-Mangostin was recorded and the IC_{50} was obtained from a Hill fit.
647 The THexA competition experiments for BKα channels were conducted as 3-point
648 determinations using 0.1 µM and 1 µM THexA as concentrations close to half-maximal
649 inhibition without and with α-Mangostin and 10 µM THexA for full block. To estimate the IC_{50},
650 a simplified 4-parameter logistic regression was used, assuming $a = 0$ and $b = 1$.

651
$$y = d + \frac{a - d}{1 + (\frac{x}{c})^b} \quad \rightarrow \quad c = \frac{x}{(\frac{d}{y} - 1)}$$

652 where *a*: lower asymptote, *b*: slope, *c*: IC_{50}, *d*: upper asymptote, *x*: THexA concentration, and
653 *y*: current.

654 *Single-channel recordings*

655 Single channels were recorded at room temperature from excised inside-out patches of
656 HEK293 cells transiently transfected with BKα in a continuous voltage protocol at +40 mV. To
657 increase the chances of obtaining patches with only one channel, a pBF vector with a
658 suboptimal beta globin promotor yielding only low expression was used. Pipette resistances
659 were 12-15 MΩ, and symmetrical intra- and extracellular solution contained (in mM) 140 KCl,
660 2 $MgCl_2$, 1 $CaCl_2$, 2.5 EGTA,10 Hepes (pH 7.3 with KOH), corresponding to ≈100 nM free Ca^{2+}.
661 Currents were recorded at a sampling rate of 100 kHz with a final bandwith f_c of 7.4 kHz using
662 an EPC10 amplifier controlled by Patchmaster software (v2.78; HEKA Elektronik, Lambrecht,
663 Germany). Traces were analyzed in Clampfit (v11.2.2.17; Molecular Devices, San Jose, USA).
664 The filter rise time $T_r = \frac{0.3321}{f_c}$ was 45 µs, and openings > 2 T_r were fitted (Colquhoun and
665 Sigworth, 1995). Histograms were calculated in Clampfit and fitted with a Gauss function to
666 obtain amplitudes and dwell times using Prism (v8.4.3; GraphPad Software Inc., San Diego,
667 USA). Single channel conductance was calculated from $g = \frac{I}{(V_m - E_{K^+})}$, where g, conductance;
668 I, single channel current; V_m, membrane voltage; E_{K+}, K^+ equilibrium potential.

669 BKα/β1 – Ca_v complexes were restored as described by (Berkefeld *et al.*, 2006) with the
670 following modification: For nanodomain formation of Ca_v 1.2 and BKα/β1, CHO-K1 cells were
671 seeded onto coverslips and microinjected (InjectMan 4, Eppendorf, Hamburg, Germany) with
672 a DNA mixture of Ca_vα 1C, Ca_v β1, Ca_v α2δ1, BKα, β1 and EYFP in the ratio 10:10:10:10:100:1
673 to ensure the presence of all subunits. Cells were incubated overnight and currents were
674 recorded from EYFP-positive cells 14-18 h after injection. Cells were measured in a
675 physiological potassium gradient with a voltage step protocol from -50 mV to +60 mV in 10 mV
676 increments. The extracellular solution contained (in mM): 135 NaCl, 5 KCl, 2 $CaCl_2$, 2 $MgCl_2$,
677 10 D(+)-glucose, 10 Hepes (pH 7.3). The intracellular solution was (in mM): 140 KCl, 2 $MgCl_2$,
678 5 EGTA, 10 Hepes (pH 7.3). α-Mangostin was added to the bath solution at a final
679 concentration of 10 µM.

680 *Molecular Docking*

681 The input structure for molecular docking was generated by truncating the structure of the
682 human BKα channel (PDB ID 6vg3) to only the pore region (res T229-R329) using PyMOL
683 (Schrodinger LLC, 2015). Docking was performed with AutoDock4 (v4.2.6) using MGL Tools
684 (v1.5.7) (Morris *et al.*, 2009). A run with lower resolution grid was done and after α-Mangostin
685 was seen in the pore, the docking was repeated with a gridbox restricted to the cavity below
686 the SF. Clustering and interactions were analyzed with the built-in functions of MGL Tools.

687 *Aortic smooth muscle preparations*

688 1 female and 7 male CD1/CHR2 mice were killed by decapitation following isoflurane-narcosis
689 and the aorta was removed. The aortic wall was dissected and tissue strips of ≈15x2 mm were
690 obtained using the spiral cut technique (Peiper and Schmidt, 1972). Aortic preparations were
691 tethered to glass holders and transferred to temperature-controlled 37 °C bath chambers filled
692 with Krebs solution (pH 7.4; in mM: 112 NaCl, 4.7 KCl, 2.5 $CaCl_2$, 1.2 $MgCl_2$, 1.2 KH_2PO_4 25
693 $NaHCO_3$ and 11.5 Glucose). The bath solution was bubbled with 95 % O_2/ 5 % CO_2. The
694 contraction force was recorded with mechanoelectric transducers (Fort100, WPI, Sarasota,
695 USA), connected to a PowerLab controlled by LabChart (AD Instruments, Mannheim,
696 Germany). A prestrain of 2.5-3.9 mN was applied, depending on the thickness of preparations,
697 and strips equilibrated for ca. 45 minutes. The NA concentration necessary to achieve half-
698 maximal contraction was determined by measuring a dose-response relationship and 100 nM
699 NA were subsequently used for precontraction. After a plateau was reached (2-4 minutes), α-
700 Mangostin and IbTx were diluted into the bath solution to their final concentrations of 10 µM
701 and 100 nM, respectively, and the contraction force was recorded for ca. 20 minutes.
702 Recordings were analyzed with LabChart.

703 *Data analysis and statistics*

704 All data are given as mean ± SEM. Mean currents were analyzed with Patchmaster (HEKA
705 Elektronik, Lambrecht, Germany). Fitmaster (HEKA Elektronik, Lambrecht, Germany) was
706 used to generate GV-relationships and fits with the Boltzmann function, and for the
707 monoexponential fits to obtain activation and deactivation time constants. EC_{50} / IC_{50} values
708 were obtained by fitting a Hill equation to the dose-response data using IgorPro (v6.3.7;
709 WaveMetrics, Portland, USA) or Prism (v8.4.3; Graphpad Software Inc., San Diego, USA).

710 $$I_0 + \frac{I_{max} - I_0}{1 + \left(\frac{c_{1/2}}{c}\right)^h}$$

711 With I_0, basal current; I_{max}, activated current; c, concentration; $c_{½}$ EC_{50} / IC_{50}; h, Hill coefficient.

712 Statistical analysis was conducted with the built-in functions of Prism. If data were not normally
713 distributed, nonparametric tests were used. Variances were compared with F-tests. Two
714 means were then compared with a paired or unpaired t-test. Three or more groups were
715 compared using one-way ANOVA when variances and standard deviation were considered
716 equal by Bartlett's test, otherwise the Brown-Forsythe and Welch ANOVA was applied.
717 Dunnett's T3 post-hoc test was used to account for multiple comparisons in ANOVA, and
718 Dunn's post-hoc test was used for non-parametric tests. Data and statistical tests are reported
719 in supplementary tables for each figure. Symbols for P values are used in the figures as follows:
720 *** (P <0.001), ** (P ≤0.01), * (P ≤0.05), ns (P ≥0. 05).

721 Structures were visualized with PyMOL (Schrodinger LLC, 2015) and figures were assembled
722 with Inkscape v1.3 (GNU General Public License, v3).

723

724 **Acknowledgements**

725 Parts of this study were supported by the DFG grant 506373940 to MM and TB.

726 Plasmids containing the BK β1 subunit and the different $Ca_v1.2$ subunits were a gift of Bernd
727 Fakler (Universität Freiburg). $K_v1.3$ was kindly provided by Heinrich Terlau (Christian-
728 Albrechts-Universität zu Kiel). GoSlo-SR-5-6 was received by courtesy of Mark Hollywood
729 (Dundalk Institute of Technology). We thank Michaela Unmack, Sandra Grüssel, Henning
730 Janssen and Petra Breiden for excellent technical assistance.

731

732 **Ethics declaration**

733 Breeding, housing and procedures to obtain aortic tissue from mice were licensed and
734 performed according to German animal protection law, the regulations of the state authorities
735 of Mecklenburg-West Pomerania, and the standards of the University of Rostock.

736 The authors declare no competing interest.

737

References

Alpha-Tocopherol, Beta Carotene Cancer Prevention Study Group (1994) "The effect of vitamin E and beta carotene on the incidence of lung cancer and other cancers in male smokers," *The New England Journal of Medicine*, 330(15), pp. 1029–1035. Available at: https://doi.org/10.1056/NEJM199404143301501.

Barenco-Marins, T.S. *et al.* (2023) "Pulmonary Circulation Under Pressure: Pathophysiological and Therapeutic Implications of BK Channel," *Cardiovascular Drugs and Therapy* [Preprint]. Available at: https://doi.org/10.1007/s10557-023-07503-7.

Bentzen, B.H. *et al.* (2014) "BK channel activators and their therapeutic perspectives," *Frontiers in Physiology*, 5. Available at: https://www.frontiersin.org/articles/10.3389/fphys.2014.00389 (Accessed: April 17, 2023).

Berkefeld, H. *et al.* (2006) "BKCa-Cav Channel Complexes Mediate Rapid and Localized Ca2+-Activated K+ Signaling," *Science*, 314(5799), pp. 615–620. Available at: https://doi.org/10.1126/science.1132915.

Berkefeld, H. and Fakler, B. (2008) "Repolarizing Responses of BKCa–Cav Complexes Are Distinctly Shaped by Their Cav Subunits," *Journal of Neuroscience*, 28(33), pp. 8238–8245. Available at: https://doi.org/10.1523/JNEUROSCI.2274-08.2008.

Berkefeld, H., Fakler, B. and Schulte, U. (2010) "Ca2+-Activated K+ Channels: From Protein Complexes to Function," *Physiological Reviews*, 90(4), pp. 1437–1459. Available at: https://doi.org/10.1152/physrev.00049.2009.

Bobak, N. *et al.* (2017) "Recombinant tandem of pore-domains in a Weakly Inward rectifying K+ channel 2 (TWIK2) forms active lysosomal channels.," *Scientific Reports*, 7(1), p. 649. Available at: https://doi.org/10.1038/s41598-017-00640-8.

Brenner, R. *et al.* (2000) "Vasoregulation by the β1 subunit of the calcium-activated potassium channel," *Nature*, 407(6806), pp. 870–876. Available at: https://doi.org/10.1038/35038011.

Brown, K. *et al.* (2024) "Resveratrol for the Management of Human Health: How Far Have We Come? A Systematic Review of Resveratrol Clinical Trials to Highlight Gaps and Opportunities," *International Journal of Molecular Sciences*, 25(2), p. 747. Available at: https://doi.org/10.3390/ijms25020747.

Câmara, D.V. *et al.* (2010) "Mechanism of the vasodilator effect of Euxanthone in rat small mesenteric arteries," *Phytomedicine*, 17(8), pp. 690–692. Available at: https://doi.org/10.1016/j.phymed.2009.12.003.

Capettini, L.S.A. *et al.* (2009) "Vasodilator and Antioxidant Effect of Xanthones Isolated from Brazilian Medicinal Plants," *Planta Medica*, 75(02), pp. 145–148. Available at: https://doi.org/10.1055/s-0028-1088388.

Chairungsrilerd, N. *et al.* (1996) "Pharmacological properties of alpha-mangostin, a novel histamine H1 receptor antagonist," *European Journal of Pharmacology*, 314(3), pp. 351–356. Available at: https://doi.org/10.1016/s0014-2999(96)00562-6.

Chairungsrilerd, N. *et al.* (1997) "γ-Mangostin, a novel type of 5-hydroxytryptamine 2A receptor antagonist," *Naunyn-Schmiedeberg's Archives of Pharmacology*, 357(1), pp. 25–31. Available at: https://doi.org/10.1007/PL00005134.

Chen, J., Seebohm, G. and Sanguinetti, M.C. (2002) “Position of aromatic residues in the S6 domain, not inactivation, dictates cisapride sensitivity of HERG and eag potassium channels.,” *Proceedings of the National Academy of Sciences of the United States of America*, 99(19), pp. 12461–12466. Available at: https://doi.org/10.1073/pnas.192367299.

Chen, X., Yan, J. and Aldrich, R.W. (2014) “BK channel opening involves side-chain reorientation of multiple deep-pore residues,” *Proceedings of the National Academy of Sciences*, 111(1), pp. E79–E88. Available at: https://doi.org/10.1073/pnas.1321697111.

Cheng, Y.-W. and Kang, J.-J. (1997) “Mechanism of vasorelaxation of thoracic aorta caused by xanthone,” *European Journal of Pharmacology*, 336(1), pp. 23–28. Available at: https://doi.org/10.1016/S0014-2999(97)01224-7.

Clay, J.R. (2017) “Novel description of the large conductance Ca2+-modulated K+ channel current, BK, during an action potential from suprachiasmatic nucleus neurons,” *Physiological Reports*, 5(20), p. e13473. Available at: https://doi.org/10.14814/phy2.13473.

Colquhoun, D. and Sigworth, F.J. (1995) “Fitting and Statistical Analysis of Single-Channel Records,” in B. Sakmann and E. Neher (eds.) *Single-Channel Recording*. 2nd ed. Boston, MA: Springer US, pp. 483–587. Available at: https://doi.org/10.1007/978-1-4615-7858-1_11.

Cui, J., Cox, D.H. and Aldrich, R.W. (1997) “Intrinsic Voltage Dependence and Ca2+ Regulation of mslo Large Conductance Ca-activated K+ Channels,” *Journal of General Physiology*, 109(5), pp. 647–673. Available at: https://doi.org/10.1085/jgp.109.5.647.

Di Pierro, F. *et al.* (2023) “Quercetin as a possible complementary agent for early-stage COVID-19: Concluding results of a randomized clinical trial,” *Frontiers in Pharmacology*, 13. Available at: https://doi.org/10.3389/fphar.2022.1096853.

Diniz, T.F. *et al.* (2013) “Mechanism of the Vasodilator Effect of Mono-oxygenated Xanthones: A Structure-Activity Relationship Study,” *Planta Medica*, 79(16), pp. 1495–1500. Available at: https://doi.org/10.1055/s-0033-1350803.

Dudem, S. *et al.* (2020) “LINGO1 is a regulatory subunit of large conductance, Ca2+-activated potassium channels,” *Proceedings of the National Academy of Sciences*, 117(4), pp. 2194–2200. Available at: https://doi.org/10.1073/pnas.1916715117.

Dworetzky, S.I. *et al.* (1996) “Phenotypic alteration of a human BK (hSlo) channel by hSlobeta subunit coexpression: changes in blocker sensitivity, activation/relaxation and inactivation kinetics, and protein kinase A modulation,” *The Journal of Neuroscience: The Official Journal of the Society for Neuroscience*, 16(15), pp. 4543–4550. Available at: https://doi.org/10.1523/JNEUROSCI.16-15-04543.1996.

Eisvand, F. *et al.* (2022) “Cardioprotective effects of alpha-mangostin on doxorubicin-induced cardiotoxicity in rats,” *Phytotherapy Research*, 36(1), pp. 506–524. Available at: https://doi.org/10.1002/ptr.7356.

Fan, C. *et al.* (2023) “Calcium-gated potassium channel blockade via membrane-facing fenestrations,” *Nature Chemical Biology*, pp. 1–10. Available at: https://doi.org/10.1038/s41589-023-01406-2.

Feliciangeli, S. *et al.* (2010) “Potassium channel silencing by constitutive endocytosis and intracellular sequestration.,” *The Journal of Biological Chemistry*, 285(7), pp. 4798–805. Available at: https://doi.org/10.1074/jbc.M109.078535.

Ferraguto, C. *et al.* (2024) “Therapeutic efficacy of the BKCa channel opener chlorzoxazone in a mouse model of Fragile X syndrome,” *Neuropsychopharmacology: Official Publication of the American College of Neuropsychopharmacology*, 49(13), pp. 2032–2041. Available at: https://doi.org/10.1038/s41386-024-01956-6.

Giangiacomo, K.M. *et al.* (1998) “Mechanism of Maxi-K Channel Activation by Dehydrosoyasaponin-I,” *Journal of General Physiology*, 112(4), pp. 485–501. Available at: https://doi.org/10.1085/jgp.112.4.485.

Gierten, J. *et al.* (2008) “Regulation of two-pore-domain (K2P) potassium leak channels by the tyrosine kinase inhibitor genistein.,” *British Journal of Pharmacology*, 154(8), pp. 1680–90. Available at: https://doi.org/10.1038/bjp.2008.213.

Gonzalez-Perez, V. and Lingle, C.J. (2019) “Regulation of BK Channels by Beta and Gamma Subunits,” *Annual review of physiology*, 81, pp. 113–137. Available at: https://doi.org/10.1146/annurev-physiol-022516-034038.

Gonzalez-Sanabria, N. *et al.* (2025) “The BK channel-NS1619 agonist complex reveals molecular insights on allosteric activation gating.” bioRxiv, p. 2025.03.27.645783. Available at: https://doi.org/10.1101/2025.03.27.645783.

Gu, R.-X. and de Groot, B.L. (2023) “Central cavity dehydration as a gating mechanism of potassium channels,” *Nature Communications*, 14(1), p. 2178. Available at: https://doi.org/10.1038/s41467-023-37531-8.

Han, S.Y. *et al.* (2015) “Dose-Independent ADME Properties and Tentative Identification of Metabolites of α-Mangostin from Garcinia mangostana in Mice by Automated Microsampling and UPLC-MS/MS Methods,” *PLOS ONE*, 10(7), p. e0131587. Available at: https://doi.org/10.1371/journal.pone.0131587.

Hanner, M. *et al.* (1997) “The beta subunit of the high-conductance calcium-activated potassium channel contributes to the high-affinity receptor for charybdotoxin,” *Proceedings of the National Academy of Sciences of the United States of America*, 94(7), pp. 2853–2858. Available at: https://doi.org/10.1073/pnas.94.7.2853.

Hennekens, C.H. *et al.* (1996) “Lack of effect of long-term supplementation with beta carotene on the incidence of malignant neoplasms and cardiovascular disease,” *The New England Journal of Medicine*, 334(18), pp. 1145–1149. Available at: https://doi.org/10.1056/NEJM199605023341801.

Hill-Eubanks, D.C. *et al.* (2011) “Calcium signaling in smooth muscle,” *Cold Spring Harbor Perspectives in Biology*, 3(9), p. a004549. Available at: https://doi.org/10.1101/cshperspect.a004549.

Hite, R.K., Tao, X. and MacKinnon, R. (2017) “Structural basis for gating the high-conductance Ca(2+)-activated K(+) channel.,” *Nature*, 541(7635), pp. 52–57. Available at: https://doi.org/10.1038/nature20775.

Horrigan, F.T. and Aldrich, R.W. (2002) “Coupling between voltage sensor activation, Ca2+ binding and channel opening in large conductance (BK) potassium channels,” *The Journal of General Physiology*, 120(3), pp. 267–305. Available at: https://doi.org/10.1085/jgp.20028605.

Hoshi, T., Xu, R., *et al.* (2013) “A point mutation in the human Slo1 channel that impairs its sensitivity to omega-3 docosahexaenoic acid,” *Journal of General Physiology*, 142(5), pp. 507–522. Available at: https://doi.org/10.1085/jgp.201311061.

Hoshi, T., Tian, Y., *et al.* (2013) “Mechanism of the modulation of BK potassium channel complexes with different auxiliary subunit compositions by the omega-3 fatty acid DHA,” *Proceedings of the National Academy of Sciences*, 110(12), pp. 4822–4827. Available at: https://doi.org/10.1073/pnas.1222003110.

Hoshi, T. and Heinemann, S.H. (2016) “Modulation of BK Channels by Small Endogenous Molecules and Pharmaceutical Channel Openers.,” *International Review of Neurobiology*, 128, pp. 193–237. Available at: https://doi.org/10.1016/bs.irn.2016.03.020.

Jang, M. *et al.* (1997) “Cancer chemopreventive activity of resveratrol, a natural product derived from grapes,” *Science (New York, N.Y.)*, 275(5297), pp. 218–220. Available at: https://doi.org/10.1126/science.275.5297.218.

Jia, Z. *et al.* (2018) “Hydrophobic gating in BK channels,” *Nature Communications*, 9(1), p. 3408. Available at: https://doi.org/10.1038/s41467-018-05970-3.

John, O.D. *et al.* (2022) “The metabolic and molecular mechanisms of α-mangostin in cardiometabolic disorders (Review),” *International Journal of Molecular Medicine*, 50(3), p. 120. Available at: https://doi.org/10.3892/ijmm.2022.5176.

Kim, E.-J., Kang, D. and Han, J. (2011) “Baicalein and wogonin are activators of rat TREK-2 two-pore domain K+ channel,” *Acta Physiologica (Oxford, England)*, 202(2), pp. 185–192. Available at: https://doi.org/10.1111/j.1748-1716.2011.02263.x.

Kim, H.J. *et al.* (2021) “Inhibitory effects of α-Mangostin on T cell cytokine secretion via ORAI1 calcium channel and K+ channels inhibition,” *PeerJ*, 9, p. e10973. Available at: https://doi.org/10.7717/peerj.10973.

Kim, S.E. *et al.* (2023) “Multi-target modulation of ion channels underlying the analgesic effects of α-mangostin in dorsal root ganglion neurons,” *Phytomedicine*, 115, p. 154791. Available at: https://doi.org/10.1016/j.phymed.2023.154791.

Knaus, H.G. *et al.* (1994) “Subunit composition of the high conductance calcium-activated potassium channel from smooth muscle, a representative of the mSlo and slowpoke family of potassium channels,” *The Journal of Biological Chemistry*, 269(6), pp. 3921–3924.

Kondo, M. *et al.* (2009) “Bioavailability and Antioxidant Effects of a Xanthone-Rich Mangosteen (Garcinia mangostana) Product in Humans,” *Journal of Agricultural and Food Chemistry*, 57(19), pp. 8788–8792. Available at: https://doi.org/10.1021/jf901012f.

Kong, C., Jia, L. and Jia, J. (2022) “γ-mangostin attenuates amyloid-β42-induced neuroinflammation and oxidative stress in microglia-like BV2 cells via the mitogen-activated protein kinases signaling pathway,” *European Journal of Pharmacology*, 917, p. 174744. Available at: https://doi.org/10.1016/j.ejphar.2022.174744.

Large, R.J. *et al.* (2015) “Effects of the novel BK (KCa1.1) channel opener GoSlo-SR-5-130 are dependent on the presence of BKβ subunits,” *British Journal of Pharmacology*, 172(10), pp. 2544–2556. Available at: https://doi.org/10.1111/bph.13085.

Latorre, R. *et al.* (2017) “Molecular Determinants of BK Channel Functional Diversity and Functioning,” *Physiological Reviews*, 97(1), pp. 39–87. Available at: https://doi.org/10.1152/physrev.00001.2016.

Lee, S. *et al.* (2021) “Virus-induced senescence is a driver and therapeutic target in COVID-19,” *Nature*, 599(7884), pp. 283–289. Available at: https://doi.org/10.1038/s41586-021-03995-1.

Li, Q. and Yan, J. (2016) “Modulation of BK Channel Function by Auxiliary Beta and Gamma Subunits,” *International review of neurobiology*, 128, pp. 51–90. Available at: https://doi.org/10.1016/bs.irn.2016.03.015.

Li, R. *et al.* (2019) “Alpha-Mangostin Ameliorates Bleomycin-Induced Pulmonary Fibrosis in Mice Partly Through Activating Adenosine 5’-Monophosphate-Activated Protein Kinase,” *Frontiers in Pharmacology*, 10, p. 1305. Available at: https://doi.org/10.3389/fphar.2019.01305.

Li, W. and Aldrich, R.W. (2004) “Unique Inner Pore Properties of BK Channels Revealed by Quaternary Ammonium Block,” *Journal of General Physiology*, 124(1), pp. 43–57. Available at: https://doi.org/10.1085/jgp.200409067.

Magleby, K.L. (2003) “Gating mechanism of BK (Slo1) channels: so near, yet so far,” *The Journal of General Physiology*, 121(2), pp. 81–96. Available at: https://doi.org/10.1085/jgp.20028721.

Majdalawieh, A.F. *et al.* (2024) “α-Mangostin: A Xanthone Derivative in Mangosteen with Potent Anti-Cancer Properties,” *Biomolecules*, 14(11), p. 1382. Available at: https://doi.org/10.3390/biom14111382.

Martín, P. *et al.* (2021) “Arachidonic acid effect on the allosteric gating mechanism of BK (Slo1) channels associated with the β1 subunit,” *Biochimica et Biophysica Acta (BBA) - Biomembranes*, 1863(9), p. 183550. Available at: https://doi.org/10.1016/j.bbamem.2021.183550.

McManus, O.B. *et al.* (1993) “An activator of calcium-dependent potassium channels isolated from a medicinal herb,” *Biochemistry*, 32(24), pp. 6128–6133. Available at: https://doi.org/10.1021/bi00075a002.

McManus, O.B. *et al.* (1995) “Functional role of the beta subunit of high conductance calcium-activated potassium channels,” *Neuron*, 14(3), pp. 645–650. Available at: https://doi.org/10.1016/0896-6273(95)90321-6.

Morris, G.M. *et al.* (2009) “AutoDock4 and AutoDockTools4: Automated Docking with Selective Receptor Flexibility,” *Journal of computational chemistry*, 30(16), pp. 2785–2791. Available at: https://doi.org/10.1002/jcc.21256.

Nardi, A. and Olesen, S.-P. (2008) “BK Channel Modulators: A Comprehensive Overview,” *Current Medicinal Chemistry*, 15(11), pp. 1126–1146. Available at: https://doi.org/10.2174/092986708784221412.

National Center for Biotechnology Information (2025) *PubChem Compound Summary for CID 5281650, Mangostin*. Available at: https://pubchem.ncbi.nlm.nih.gov/compound/Mangostin (Accessed: October 2, 2025).

Nordquist, E.B., Jia, Z. and Chen, J. (2024) “Small Molecule NS11021 Promotes BK Channel Activation by Increasing Inner Pore Hydration,” *Journal of Chemical Information and Modeling*, 64(19), pp. 7616–7625. Available at: https://doi.org/10.1021/acs.jcim.4c01012.

Orio, P. and Latorre, R. (2005) “Differential Effects of β1 and β2 Subunits on BK Channel Activity,” *The Journal of General Physiology*, 125(4), pp. 395–411. Available at: https://doi.org/10.1085/jgp.200409236.

940 Peiper, U. and Schmidt, E. (1972) “Relaxation of coronary arteries by electro-mechanical decoupling
941 or adrenergic stimulation,” *Pflugers Archiv: European Journal of Physiology*, 337(2), pp. 107–117.
942 Available at: https://doi.org/10.1007/BF00587834.

943 Pereira da Silva, E.A. *et al.* (2022) “Ion channel molecular complexes in vascular smooth muscle,”
944 *Frontiers in Physiology*, 13, p. 999369. Available at: https://doi.org/10.3389/fphys.2022.999369.

945 Petiwala, S.M. *et al.* (2014) “Pharmacokinetic characterization of mangosteen (Garcinia mangostana)
946 fruit extract standardized to α-mangostin in C57BL/6 mice,” *Nutrition Research*, 34(4), pp. 336–345.
947 Available at: https://doi.org/10.1016/j.nutres.2014.03.002.

948 Piechotta, P.L. *et al.* (2011) “The pore structure and gating mechanism of K2P channels.,” *The EMBO*
949 *Journal*, 30(17), pp. 3607–19. Available at: https://doi.org/10.1038/emboj.2011.268.

950 Piskorowski, R.A. and Aldrich, R.W. (2006) “Relationship between pore occupancy and gating in BK
951 potassium channels.,” *The Journal of General Physiology*, 127(5), pp. 557–576. Available at:
952 https://doi.org/10.1085/jgp.200509482.

953 Ramaiya, A. *et al.* (2012) “Single Dose Oral Pharmacokinetic Profile of α-Mangostin in Mice,” *Current*
954 *Drug Targets*, 13(14), pp. 1698–1704. Available at: https://doi.org/10.2174/138945012804545524.

955 Richter-Laskowska, M. *et al.* (2023) “Flavonoids as Modulators of Potassium Channels,” *International*
956 *Journal of Molecular Sciences*, 24(2), p. 1311. Available at: https://doi.org/10.3390/ijms24021311.

957 Rockman, M.E., Vouga, A.G. and Rothberg, B.S. (2020a) “Molecular mechanism of BK channel
958 activation by the smooth muscle relaxant NS11021,” *Journal of General Physiology*, 152(6), p.
959 e201912506. Available at: https://doi.org/10.1085/jgp.201912506.

960 Rockman, M.E., Vouga, A.G. and Rothberg, B.S. (2020b) “Molecular mechanism of BK channel
961 activation by the smooth muscle relaxant NS11021,” *The Journal of General Physiology*, 152(6), p.
962 e201912506. Available at: https://doi.org/10.1085/jgp.201912506.

963 Roy, S. *et al.* (2012) “Structure–Activity Relationships of a Novel Group of Large-Conductance Ca2+-
964 Activated K+ (BK) Channel Modulators: The GoSlo-SR Family,” *ChemMedChem*, 7(10), pp. 1763–1769.
965 Available at: https://doi.org/10.1002/cmdc.201200321.

966 Savineau, J.-P. and Marthan, R. (2000) “Cytosolic Calcium Oscillations in Smooth Muscle Cells,”
967 *Physiology*, 15(1), pp. 50–55. Available at: https://doi.org/10.1152/physiologyonline.2000.15.1.50.

968 Schewe, M. *et al.* (2019) “A pharmacological master key mechanism that unlocks the selectivity filter
969 gate in K + channels.,” *Science*, 363(6429), pp. 875–880. Available at:
970 https://doi.org/10.1126/science.aav0569.

971 Schrodinger LLC (2015) *The PyMOL Molecular Graphics System, Version 1.8*.

972 Shah, K.R., Guan, X. and Yan, J. (2022) “Structural and Functional Coupling of Calcium-Activated BK
973 Channels and Calcium-Permeable Channels Within Nanodomain Signaling Complexes,” *Frontiers in*
974 *Physiology*, 12. Available at: https://doi.org/10.3389/fphys.2021.796540.

975 Sun, L. and Horrigan, F.T. (2022) “A gating lever and molecular logic gate that couple voltage and
976 calcium sensor activation to opening in BK potassium channels,” *Science Advances*, 8(50), p.
977 eabq5772. Available at: https://doi.org/10.1126/sciadv.abq5772.

Tao, X., Hite, R.K. and MacKinnon, R. (2017) “Cryo-EM structure of the open high-conductance Ca2+-activated K+ channel.,” *Nature*, 541(7635), pp. 46–51. Available at: https://doi.org/10.1038/nature20608.

Tatiya-Aphiradee, N., Chatuphonprasert, W. and Jarukamjorn, K. (2016) “In vivo antibacterial activity of Garcinia mangostana pericarp extract against methicillin-resistant Staphylococcus aureus in a mouse superficial skin infection model,” *Pharmaceutical Biology*, 54(11), pp. 2606–2615. Available at: https://doi.org/10.3109/13880209.2016.1172321.

Tep-Areenan, P. and Suksamrarn, S. (2012) “Mechanisms of vasorelaxation to gamma-mangostin in the rat aorta,” *Journal of the Medical Association of Thailand = Chotmaihet Thangphaet*, 95 Suppl 12, pp. S63-68.

Tykocki, N.R., Boerman, E.M. and Jackson, W.F. (2017) “Smooth Muscle Ion Channels and Regulation of Vascular Tone in Resistance Arteries and Arterioles,” in *Comprehensive Physiology*. John Wiley & Sons, Ltd, pp. 485–581. Available at: https://doi.org/10.1002/cphy.c160011.

Valverde, M.A. *et al.* (1999) “Acute activation of Maxi-K channels (hSlo) by estradiol binding to the beta subunit,” *Science (New York, N.Y.)*, 285(5435), pp. 1929–1931. Available at: https://doi.org/10.1126/science.285.5435.1929.

Wang, L.-W. *et al.* (2002) “Antihypertensive and vasorelaxing activities of synthetic xanthone derivatives,” *Bioorganic & Medicinal Chemistry*, 10(3), pp. 567–572. Available at: https://doi.org/10.1016/S0968-0896(01)00315-7.

Webb, T.I. *et al.* (2015) “Molecular mechanisms underlying the effect of the novel BK channel opener GoSlo: Involvement of the S4/S5 linker and the S6 segment,” *Proceedings of the National Academy of Sciences*, 112(7), pp. 2064–2069. Available at: https://doi.org/10.1073/pnas.1400555112.

Wu, R.S. and Marx, S.O. (2010) “The BK potassium channel in the vascular smooth muscle and kidney: α- and β-subunits,” *Kidney International*, 78(10), pp. 963–974. Available at: https://doi.org/10.1038/ki.2010.325.

Wu, Ying *et al.* (2009) “Intersubunit Coupling in the Pore of BK Channels,” *Journal of Biological Chemistry*, 284(35), pp. 23353–23363. Available at: https://doi.org/10.1074/jbc.M109.027789.

Xin, J. *et al.* (2022) “Association between circulating vitamin E and ten common cancers: evidence from large-scale Mendelian randomization analysis and a longitudinal cohort study,” *BMC Medicine*, 20(1), p. 168. Available at: https://doi.org/10.1186/s12916-022-02366-5.

Xu, Y. *et al.* (2024) “α-Mangostin reduces hypertension in spontaneously hypertensive rats and inhibits EMT and fibrosis in Ang II-induced HK-2 cells,” *International Journal of Medical Sciences*, 21(9), pp. 1681–1688. Available at: https://doi.org/10.7150/ijms.94236.

Zhang, G. *et al.* (2022) “An allosteric modulator activates BK channels by perturbing coupling between Ca2+ binding and pore opening,” *Nature Communications*, 13(1), p. 6784. Available at: https://doi.org/10.1038/s41467-022-34359-6.

Zhou, Y., Xia, X.-M. and Lingle, C.J. (2011) “Cysteine scanning and modification reveal major differences between BK channels and Kv channels in the inner pore region.,” *Proceedings of the National Academy of Sciences of the United States of America*, 108(29), pp. 12161–12166. Available at: https://doi.org/10.1073/pnas.1104150108.

1018 ZhuGe, R. *et al.* (2002) “Spontaneous Transient Outward Currents Arise from Microdomains Where
1019 BK Channels Are Exposed to a Mean Ca2+ Concentration on the Order of 10 µM during a Ca2+
1020 Spark,” *The Journal of General Physiology*, 120(1), pp. 15–27. Available at:
1021 https://doi.org/10.1085/jgp.20028571.

1022